2016-02-01

Inversion Characteristics of a Buoyant Cylindrical Puck During Oblique Water Impact

Zachary Crawford Smith
Brigham Young University

Inversion Characteristics of a Buoyant Cylindrical Puck During Oblique Water Impact

Zachary Crawford Snow Smith

A thesis submitted to the faculty of
Brigham Young University
in partial fulfillment of the requirements for the degree of

Master of Science

Tadd T. Truscott, Chair
R. Daniel Maynes
Julie Crockett

Department of Mechanical Engineering

Brigham Young University

February 2016

ABSTRACT

Inversion Characteristics of a Buoyant Cylindrical
Puck During Oblique Water Impact

Zachary Crawford Snow Smith
Department of Mechanical Engineering, BYU
Master of Science

The Apollo Command Module had a tendency to flip over upon impact with the ocean surface after returning from space (9/19 times). In an effort to better characterize the inversion process for future water landing vehicles, experimental results for a simplified buoyant cylindrical puck impacting the water surface are presented. This study focuses on the dependence of inversion upon vertical velocity, horizontal velocity, and the pitch angle of the puck relative to the free surface. High-speed images reveal an asymmetric cavity that forms upon water impact. The asymmetric cavity then collapses, applying a moment, which can be sufficient to invert the puck after impact. Increasing the vertical velocity increases the likelihood of inversion. The puck never flipped over below a vertical velocity of 3.75 m/s. Increasing the horizontal velocity also slightly increases the likelihood of inversion. However, the largest effect of increasing horizontal velocity is to shift the range of impact angles for which the puck will invert to lower angles. The buoyant cylindrical puck used in this study requires a higher Froude number (4.34) to invert than previous geometries which have been studied.

Keywords: Apollo, splashdown, inversion, water impact, water entry, buoyancy, water jet, jet impingement

ACKNOWLEDGMENTS

I would like to thank Dr. Tadd Truscott for his support and guidance throughout this project. I received a great deal of support from a number of the faculty and staff in the BYU Department of Mechanical Engineering. I would like to specifically acknowledge the help of Kevin Cole who was instrumental in the completion of the experimental setup.

I would also like to thank Sam Hayden and the other members of the Splash Lab for offering their assistance and advice throughout this project. Finally, I would like to thank my wife, Joanna, for her support and patience during stressful times.

TABLE OF CONTENTS

LIST OF TABLES

LIST OF FIGURES

NOMENCLATURE

α	Maximum angle reached before returning to an upright orientation
β	Trajectory angle
C_g	Center of gravity
D	Diameter of the capsule
F_D	Drag force
F_G	Force due to gravity
F_H	Hydrostatic force
F_J	Force from the jet of the collapsing cavity
F_M	Force from momentum transfer
Fr	Froude number
g	Acceleration of gravity
h	Drop height
θ	Pitch angle at impact
ϕ	Adjusted impact angle
M	Mass
M_a	Added mass
R	Radius of the capsule
ρ	density
$TiME$	Titan Mare Explorer
V_h	Horizontal velocity at impact
V_i	Total magnitude of the velocity at impact
V_v	Vertical velocity at impact
ζ	coefficient for relative importance of trajectory angle

CHAPTER 1. INTRODUCTION

Splashdown is a common way of returning spacecraft to the Earth's surface [1]. This method was adopted for the Apollo missions because a water landing provides a relatively forgiving impact for onboard equipment and astronauts as well as a large landing area. In the past, the Apollo space capsule was thoroughly tested to ensure a safe landing. During these tests, two stable floating positions were identified. One was upright in the water (referred to as Stable I), while the other was upside down in the water (referred to as Stable II) (see Figure 1.1). Under certain landing conditions the space capsule had the potential to invert after water impact. This inverted orientation hindered the process of getting the astronauts out of the capsule because the vehicle hatch was left submerged underwater. A successful solution to the problem of inversion was identified in deploying airbags to flip the capsule back to an upright position if it inverted upon impact.

The precise cause of inversion was not known at the time that these tests took place. However, forty years later, inspection of this footage resulted in a proposed cause of inversion [3]. A cavity is formed as the space capsule impacts the water. As the cavity collapses a jet is formed and impacts one side of the capsule. This jet applies a moment to the capsule which has the potential to flip it over. Despite the challenges that inversion causes, relatively few of the design parameters that affect inversion have been experimentally tested. At the time of the Apollo missions it was more cost effective to focus efforts on a way to flip the capsule back to an upright position after it inverted rather than preventing the capsule from inverting in the first place.

To date, a full understanding of the parameters that affect inversion has not yet been achieved. One of the reasons a complete study has not been attempted is that during the Apollo missions the problem of inversion was identified after the space capsule had already been designed. The parachute system, shape of the capsule, density of the capsule, and the center of mass of the capsule were defined prior to any consideration to prevent inversion. For instance, with two

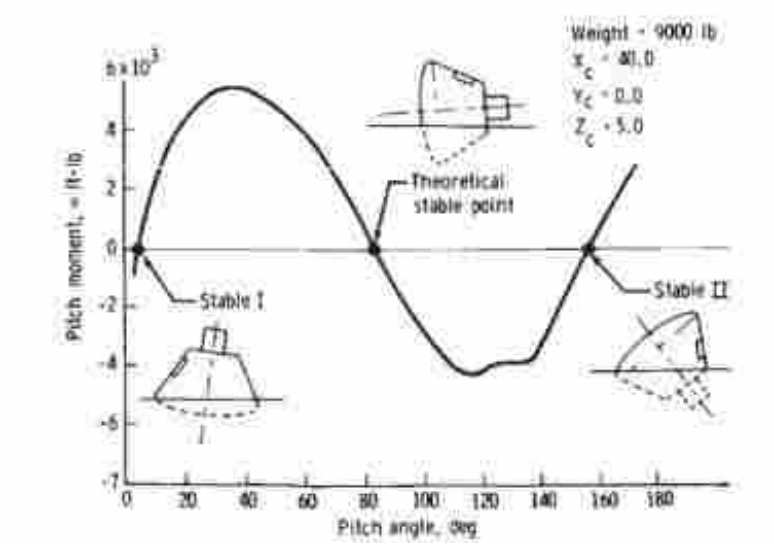

Figure 1.1: Stability curve for the Apollo command module floating in water. Two preferred stable points are shown for which the command module is in steady equilibrium (Stable I and Stable II). A third, theoretical stability point is shown ($\sim 80^\circ$) for which the command module is in unsteady equilibrium [2].

parachutes deployed it was known that the Apollo command module would fall at a terminal velocity of 10.3 m/s and with 3 parachutes deployed the command module would fall at 8.5 m/s [4]. As a result, experimental tests typically only included these two impact velocities. No tests were performed to determine the minimum impact velocity at which inversion occured. This limited the potential solutions to this problem to designs that could be fit retroactively to a completed model.

This problem has recently gained interest again due to a proposed NASA mission to Saturn's moon Titan [5]. A space probe landing on Titan will have to land in a sea of hydrocarbons and it would be advantageous to accurately predict the ultimate orientation of the probe. If the probe is guaranteed to remain upright, a mechanism to flip the probe back over would be unnecessary. Deploying airbags to flip the capsule back over proved to be successful for the Apollo missions; however, in order to facilitate future development of water landing vehicles, a more complete model of the parameters that affect inversion is essential.

1.1 Background

The general problem of water impact has been of great interest since the early 1900s. Worthington was the first to capture high-speed photography of both the splash and cavity that form

during water entry [6]. The jet that forms as a result of the collapsing cavity has come to be known as the ”Worthington jet”. During water landing of a buoyant object, a similar phenomenon takes place in which the collapsing cavity transfers energy directly to the object (see Figure 1.2). The most current research has proposed that this collapsing cavity is a cause of inversion [3]. However, high-speed video from our work shows a slightly different mechanism. As illustrated in Figure 1.2 the cavity collapses on the right side of the puck (100 ms), but does not converge to a singular point as is typical in a Worthington jet. Rather, the resulting jet impinges on the side of the puck and applies a moment, which flips the puck to an inverted orientation.

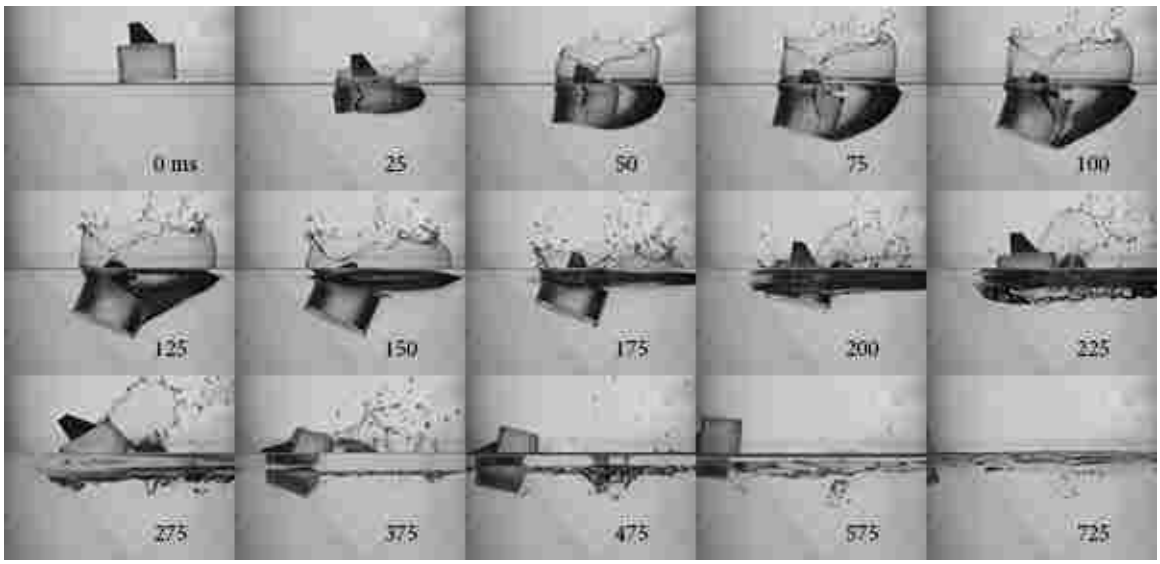

Figure 1.2: Inversion sequence for a buoyant cylindrical puck. An asymmetrical cavity forms around the puck 25-100 ms. This cavity collapses (125 - 175 ms) on the right side of the puck, but does not converge to a singular point as is typical in a Worthington jet. Rather, the resulting jet impinges on the side of the puck and applies a moment which flips the puck to an inverted orientation. At 725 ms the puck has passed it's 90° stability point and will continue to fall to an inverted orientation.

Worthington laid a foundation upon which many others began to build. The dynamic forces of water impact were closely examined to ensure a safe landing of seaplanes in the early 20th century. In 1929 Von Kármán developed a mathematical model to describe the initial impact of seaplane floats [7]. He was able to develop a model that agreed with experimental data for a vertical impact of a triangular wedge. Several other researchers added upon Von Kármán's work and in 1952 Milwitzky summarized what had been accomplished in the area of seaplane water landing

and also modified Von Kármán's solution to better fit a variety of landing conditions including limited cases of oblique water entry [8].

Milwitzky's work was further expounded upon during Project Mercury. The goal of Project Mercury was to put a human into orbit around the earth. McGehee along with the Langley Research Center modified the Von Kármán equations to form a mathematical prediction for water impact of the proposed Mercury re-entry capsule [9]. These equations showed strong agreement with 1/12 scale experimental tests for impact conditions which were both vertical and symmetrical. It was determined that this solution would be sufficient for their needs; however, it was only valid for the initial impact and offered no additional information to characterize moments applied during cavity collapse.

The final design of the Mercury re-entry capsule included airbags below the re-entry capsule that were inflated after parachute deployment and before water impact. These airbags reduced the water impact loads on the structure of the capsule. After the conclusion of Project Mercury the United States initiated a second human spaceflight program, Project Gemini. Experimental testing [10] indicated that the airbag underneath the re-entry capsule would be unnecessary if the pitch angle at impact was high enough to act as a wedge. Thompson would later expound upon this work by including rough water landing characteristics in 1967 [11].

The Apollo space program was the next challenge undertaken by NASA. During the Apollo space program, water landing was the method used to return the space craft to the earth's surface (see Figure 1.3). Inversion was recognized as a problem during early testing of water landing. Many of the tests that were performed were recorded with video [4, 10, 12]. There are even cases in which inversion is not noted in the report, but is seen in the test footage [10]. A simple solution was identified in deploying airbags that could flip the space capsule back into its Stable I position if it landed in Stable II [4]. Out of the 19 total Apollo capsules that landed in the ocean, nine inverted after impact.

In 1966, Benson summarized what was known about water landing of the Apollo command module [2]. He identified problems with using the modified Von Kármán equations to simulate water impact. The theory was limited to vertical impacts of simple geometry with known equations for added mass. The majority of the information on the Apollo water landing was obtained through

Figure 1.3: Recovery of the Apollo 11 spacecraft. During this mission the spacecraft inverted upon splashdown. The airbags were deployed to flip the capsule back to its upright orientation. (NASA)

experimental tests for this reason. Benson also showed the validity of using scaled tests for reduced costs and simplified experiments.

Extensive experimental tests were conducted to ensure the safety of water landing. In 1967 an 11 volume study of Apollo water impact was published [13–23]. These results include mathematical modelling of impact, experimental results, and numerical computer models based upon the Apollo tests. Despite a significant understanding of the water impact of the Apollo command module, very little was known relating to inversion.

In 1967 Stubbs conducted quarter scale experiments to determine the water pressures, accelerations, and landing characteristics of the Apollo spacecraft during splashdown [12]. These tests provide the most detailed description of when inversion is likely to take place. He reported that the spacecraft had the potential to capsize after impact. He noted whether the capsule inverted after each test and found several factors which affected inversion. Inversion is affected by horizontal velocity and orientation at impact. Orientation was defined by pitch, roll, and yaw angles as

defined in Figure 1.4. Water landing was tested most extensively for a large range of pitch angles at roll angles of 0° and 180°. Limited additional cases were tested for other roll and yaw angles.

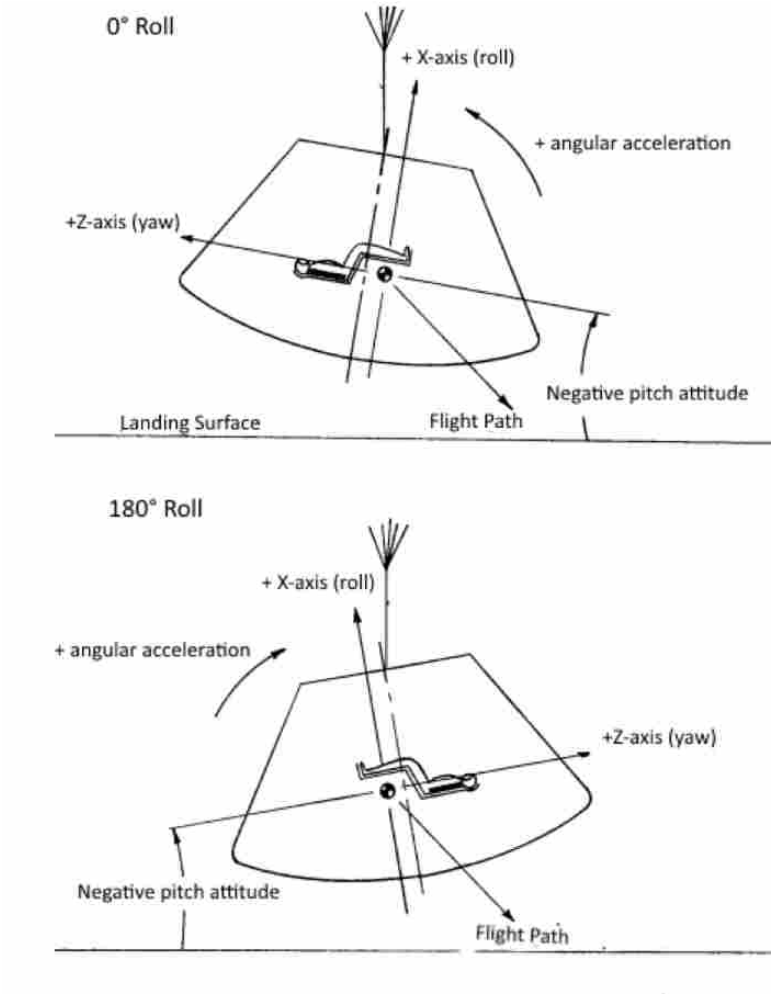

Figure 1.4: The orientation convention and geometry used in 1/4 scale experiments of the landing dynamics of the Apollo command module conducted by Sandy Stubbs. A negative pitch angle indicates a nose down orientation with 0° roll and a nose up orientation at 180° roll. The center of gravity is in front of the geometric center at 0° roll. [12]

Stubbs did not attempt a full characterization of when inversion would take place as this was beyond the scope of his study. However, he did make some observations of when inversion was likely to take place. Inversion never occured for a roll angle of 180°. This is due to the location of the center of gravity. The center of gravity of the Apollo spacecraft was off-center by 14.2 cm (5.8 in.) in the prototype of the Apollo spacecraft from which Stubbs made his model (see Figure

1.5). Inversion only occured during instances in which the center of gravity was in front of the geometric center upon water impact.

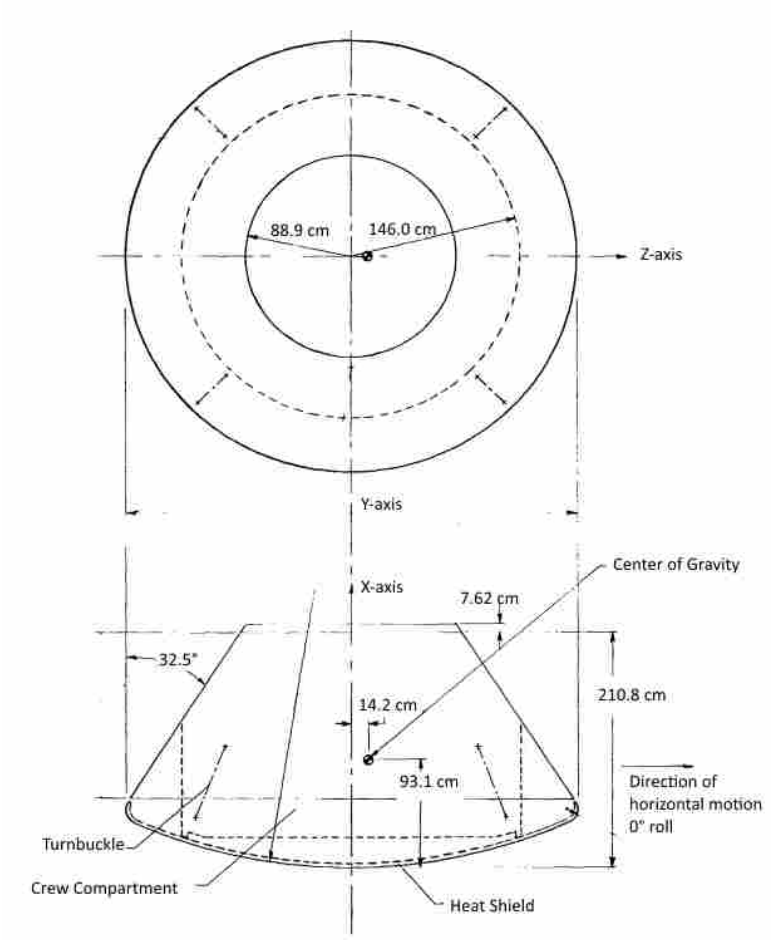

Figure 1.5: Dimensions of the prototype from which a 1/4 scale model was constructed. The center of gravity is seen to be 14.2 cm (5.8 in.) off-center horizontally and below the centerline vertically. [12]

While Stubbs did not attempt to draw many conclusions of stability from his tests, the data he provided is a valuable resource for inversion research. In Figure 1.6 a summary of Stubbs' tests are regraphed by Lorenz [3] as they relate to inversion. Two vertical velocities were tested (3.5 m/s and 4.5 m/s). Insufficient data is available for a vertical velocity of 4.5 m/s, but trends begin to appear for tests with a vertical velocity of 3.5 m/s. Increasing the horizontal velocity shifts the range of pitch angles for which the capsule is unstable upon impact. Two lines are fit to the data to show this shift. The capsule also never flipped over at a horizontal velocity of less than 2.5

m/s. Several others at this time period tested various aspects of splashdown [1]; however, none attempted a complete model of when inversion would take place.

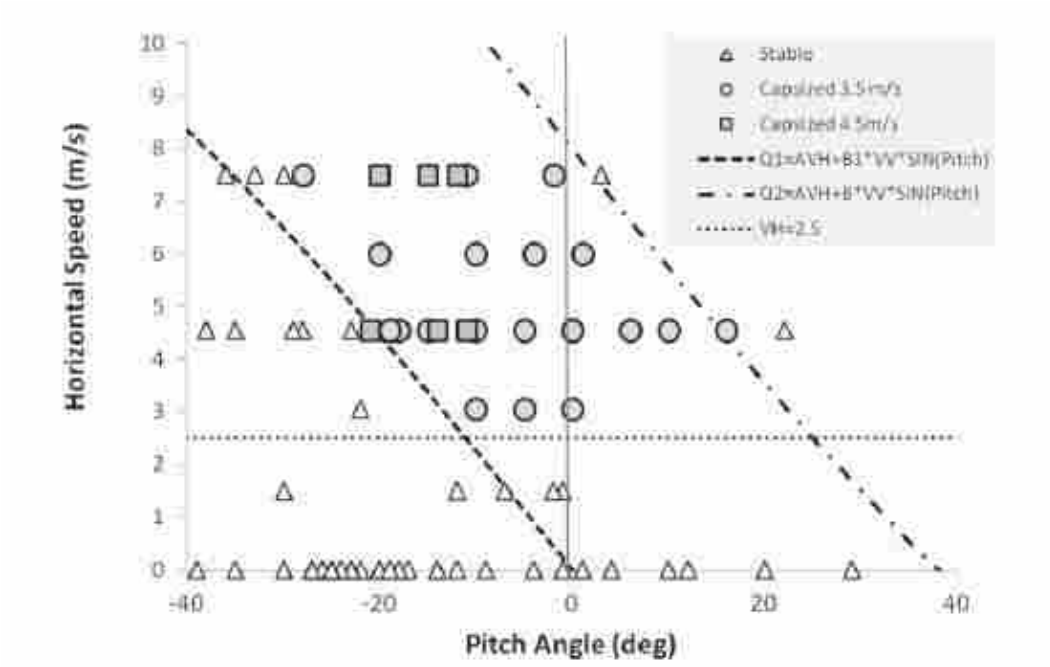

Figure 1.6: Experimental results collected by Stubbs [12] during quarter scale experiments and graphed by Lorenz [3] detailing observed conditions required for inversion. Tests resulting in inversion are marked by filled in symbols. Horizontal velocity and pitch angle at impact are both important parameters in characterizing inversion.

The most detailed explanation of inversion was given by Robert White in 1973. He reported on the command module righting system used in the Apollo missions [4]. He gave a limited set of conditions based upon empirical data for which inversion was expected (see Figure 1.7). This model proved to be unreliable as the capsule flipped over with a lower horizontal velocity than was predicted by this model. He also outlined the potential solutions that were considered by NASA to solve the problem. These potential solutions included controlling the orientation at water impact, lowering the center of mass, and including a way to flip the capsule back over while floating upside down. Ultimately, it was decided to go with a method which would deploy airbags that could flip the command module back into an upright position.

Numerical models of splashdown were developed in conjunction with the development of the Orion crew capsule [24, 25]. These models had the capability of predicting one of the

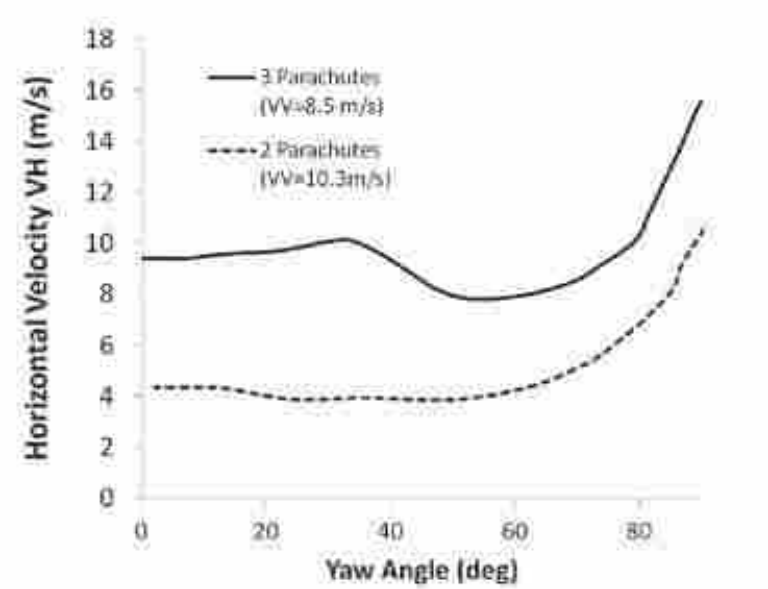

Figure 1.7: Inversion was expected for horizontal velocities above the graphed value. Tests were conducted at two vertical velocities to simulate terminal velocity at impact for both the expected case and the case in which one parachute failed to deploy. [4]

mechanisms for inversion. If the capsule came in with a high enough horizontal velocity and at the right angle, the capsule would invert due to tripping. This occurs when the front edge of the capsule catches the water and immediately inverts. Wang noted that this could occur at a pitch of -45 degrees and a horizontal velocity of 16 m/s. This is more than double the horizontal velocities that were seen causing the Apollo Capsule to invert due to a collapsing cavity underneath the capsule. These models did not capture inversion due to the collapsing cavity.

1.2 Motivation and Modern Research

In recent years the problem of inversion has resurfaced due to an interest in landing a probe on the hydrocarbon seas of Titan [5]. In 2011 Lorenz accumulated all available experimental observations for inversion and developed his own set of conditions for which inversion should be expected for the Apollo command module [3]. He used a timescale for the collapsing cavity to develop the following relation for the threshold horizontal velocity (V_t) below which inversion is not expected:

$$V_t = 0.65 L g^{5/8} \rho^{1/8} m^{-1/8} V_v^{-1/4} \tag{1.1}$$

This equation uses the assumption that the vehicle must travel some fraction of the vehicle diameter before the cavity collapses. This relationship can be expressed as $V_h = kL/\tau$. Where k is a dimensionless constant obtained through empirical data, L is the capsule diameter, and τ is the timescale for the formation and collapse of the cavity ($\tau = 2(D/g)^{0.5}$). The energy stored in the cavity is approximated to be equal to the kinetic energy of the capsule at impact.

In 2015 Lorenz expanded upon this work by presenting experimental tests (see Figure 1.8) for a 1/8 scale model of the proposed TiME capsule [26]. Two distinct criteria were established. First, below a critical horizontal velocity the capsule would not invert except under extreme impact angles. Second, the capsule also would not invert below a critical impact velocity (V_i). The resurge energy of the cavity is required to exceed the potential energy required to lift the capsule and added mass enough to flip it over by a factor γ obtained from experimental testing. The full relationship can be seen in Eqn. (1.2), where M_a is the added mass, R is the capsule radius, and M is the mass of the capsule.

$$V_i > (1 + M_a/M)(2\gamma M g R/M_a)^{0.5} \tag{1.2}$$

Their work did not expand upon the dependance upon impact angle or geometry of the impacting capsule. The assumed mechanism for inversion is described in terms of where the collapsing cavity occurs in relation to the capsule (see Figure 1.9.) If the horizontal velocity is too low, the jet impact on the capsule is too close to the center and too small of a moment is applied to the capsule to flip it over. If the horizontal velocity is near the critical velocity, the impacting jet catches the corner of the capsule flipping it over. If the horizontal velocity is too fast the jet will miss the capsule and no moment is applied.

1.3 Analogous Topics

The subject of water entry has been extensively studied [27]. Through these studies a significant amount is understood about the splash curtain, hydrodynamic forces, and cavity dynamics of a dense object entering the water. However, because these studies typically involve a dense ob-

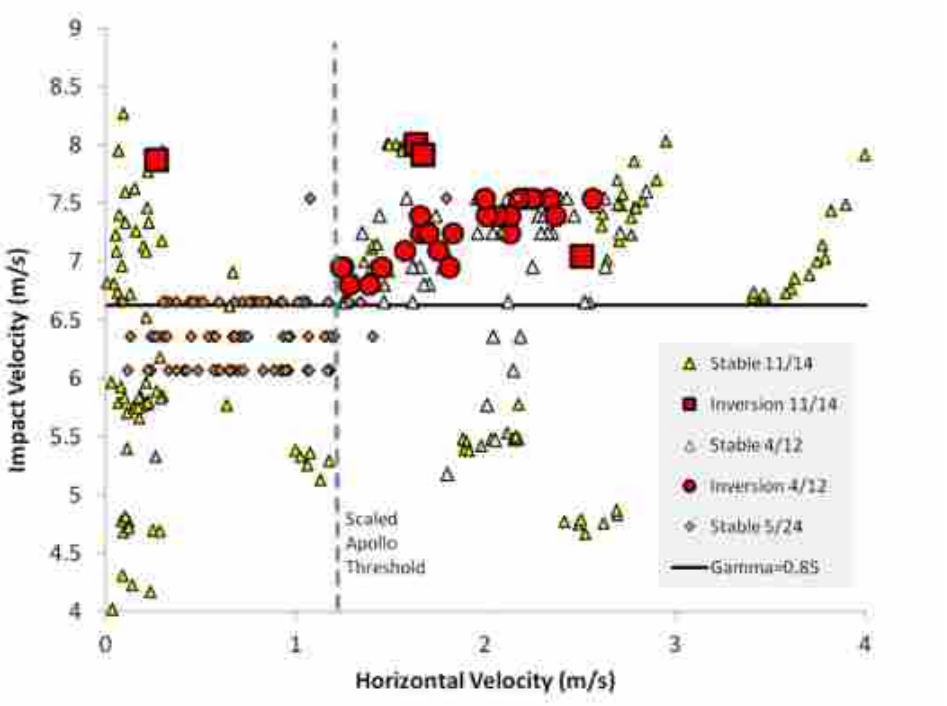

Figure 1.8: Experimental testing of a 1/8 scale model of the proposed TiME capsule. Inversion was not seen below a critical horizontal velocity or below a critical vertical velocity. One outlier indicates a test which impacted with an extreme pitch angle. [26]

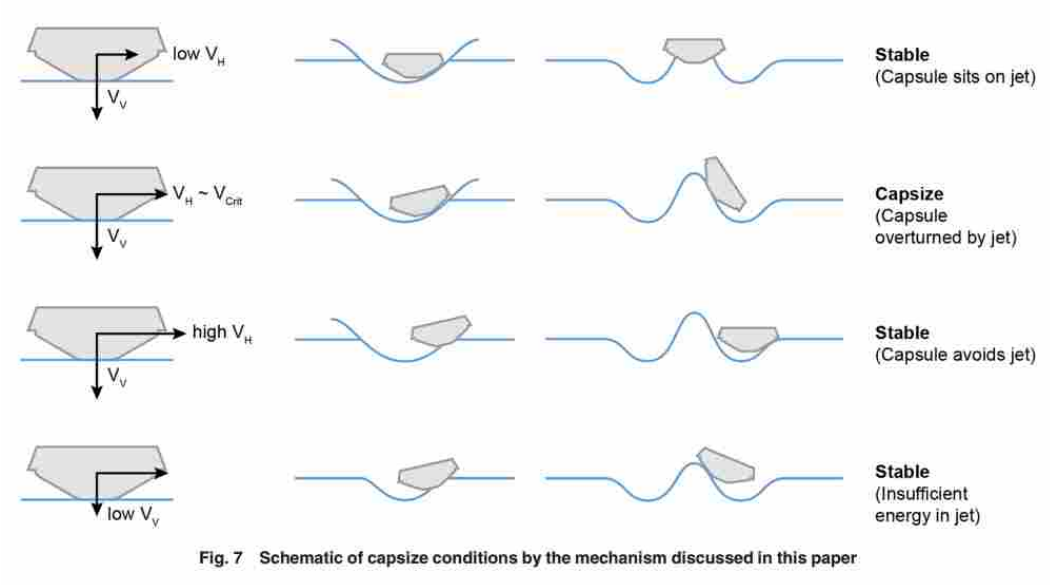

Fig. 7 Schematic of capsize conditions by the mechanism discussed in this paper

Figure 1.9: Schematic indicating the capsize conditions described by Lorenz [26]. This describes a proposed mechanism as to why the capsule required a critical horizontal and vertical velocity to invert upon impact.

ject that continues falling through the water, the cavity collapse does not directly interact with the falling object. Far less is known about the interaction between the cavity formed during water impact and a buoyant object which does not continue to descend through the water after impact [26].

A closer comparison can be drawn to a skipping stone [28] or skipping deformable sphere [29]. However, these cases differ from the present topic in that the stone or sphere leaves the cavity before collapse as is shown in Figure 1.10. Additionally, gyroscopic stability prevents inversion of a skipping stone and the orientation of a sphere is typically irrelevant. A similar skipping process was seen in numerical models of the Orion capsule landing [25]. However, this was seen at a horizontal velocity of 17 m/s which is greater than would be expected in normal landing conditions.

Figure 1.10: Image sequence for a deformable sphere skipping on water. A hydrodynamic lift force causes the sphere to leave the cavity before the cavity collapses [29].

Perhaps the closest comparison to the present topic is the study of the impact of lifeboats. In 1992 Boef presented a two part study on the launch and impact of free-fall lifeboats [30, 31]. The forces at water impact are similar to the present study. A free-body diagram can be seen in Figure 1.11. It can be seen in this figure that momentum transfer and buoyancy will apply a pitch-up moment during the initial stages of water impact. However, inversion was not a concern in this study as the lifeboat was sufficiently stable throughout the water landing process.

1.4 Objectives

The present study aims to add to the existing literature on inversion. The data available from the Apollo missions suggest a dependence upon vertical velocity, horizontal velocity, and orientation at impact. However, insufficient data was available to fully identify the trends from these experiments. Lorenz was able to identify some important trends related to vertical and horizontal velocity but does not expound upon the dependance of pitch angle at impact. There is also a

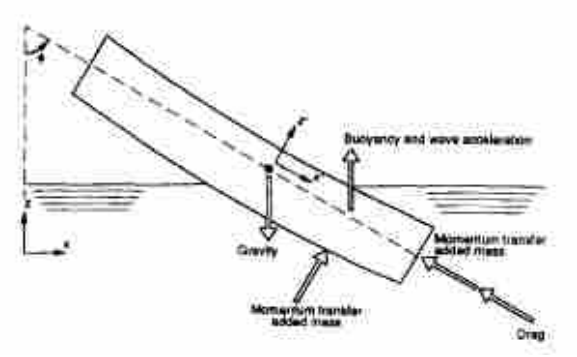

Figure 1.11: Forces on lifeboat at water entry [31].

lack in the present research of high-speed images below the water surface. These images are useful for identifying the precise cause of inversion.

In the present paper a buoyant cylindrical puck is used as a simplified representation to simulate a water landing vehicle. The dependance of inversion upon impact angle, impact velocity, and horizontal velocity is experimentally examined. High-speed video below the water surface is used to observe the process. These experiments aid in modeling the inversion phenomena, provide more accurate predictions of water landing dynamics, and make the exploration of the design space for water landing vehicles more accessible at a lower cost.

CHAPTER 2. EXPERIMENTAL METHODS

In order to better understand the inversion process, an experiment was conducted in which a buoyant cylindrical puck was dropped into a tank of water. A mechanism for dropping the pucks towards water surface was designed and built capable of controlling the horizontal velocity, vertical velocity, and pitch angle of the puck at water impact. This chapter is a summary of the experimental methods used in conducting this experiment.

2.1 Experimental Setup

A buoyant cylindrical puck was made out of acrylic for this study. Two halves of the puck were machined independently on a lathe and then attached using acetone. Dimensions are given in Figure 2.1. The puck was machined such that all sides had the same wall thickness and thus the center of gravity was directly in the center of the puck within machining error. The puck had a specific gravity of 0.41. This was calculated by measuring the mass of the puck and calculating the volume from a measured diameter and height. A small tab of aluminum foil was attached to the top to provide a simple attachment point for the release mechanism. The weight of this tab was neglected in reporting that the center of masss was directly in the center of the puck. This is justified due to the small mass of the aluminum foil relative to the rest of the puck. The aluminum foil represents less than 0.1% of the total mass.

Two separate drop mechanisms and tanks of water were used in this experiment. One setup was used for tests with a horizontal velocity. A separate setup was used for vertical drop tests with no horizontal velocity. The puck was dropped into a 61.0 x 152.4 x 91.4 cm tank of water using a custom drop mechanism that was designed and built for this experiment. The impact of the pucks with the free surface of the water was recorded at 1000 frames per second using a high-speed camera (Photron Fastcam SA3). The camera was placed perpendicular to the plane of motion and all measurements were extracted from these images. A light bank was placed behind the tank to

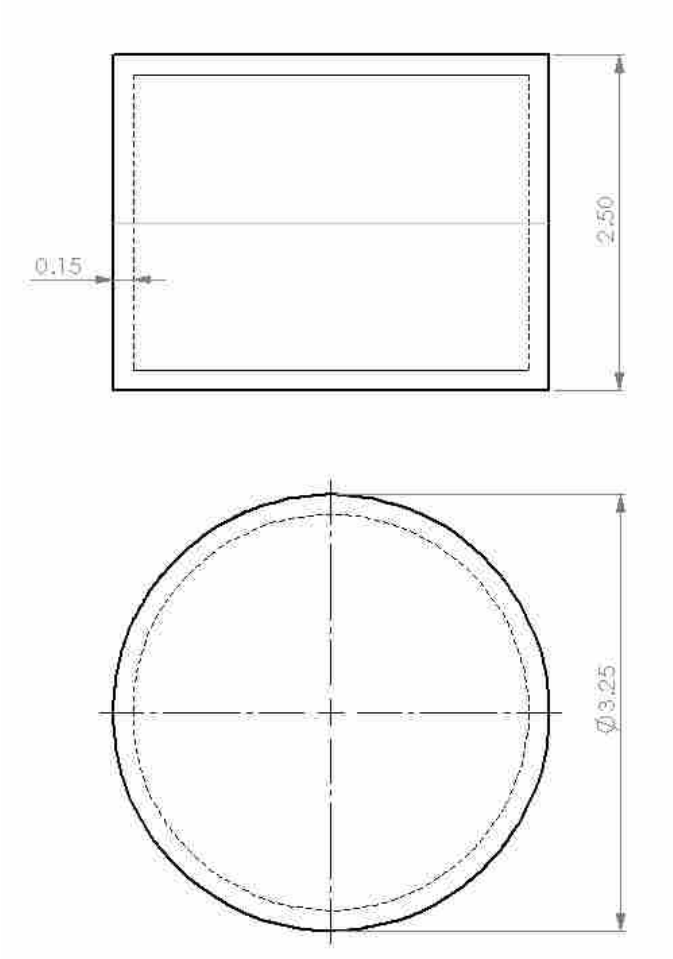

Figure 2.1: Dimensions of the acrylic puck are given in inches. The puck has the same wall thickness (0.15 inches) on every side such that the center of gravity is directly in the center of the puck.

enhance the image quality. Figure 2.2 shows a side view of the setup in which the direction of motion is into the page. Figure 2.3 shows a top view of the setup where the direction of motion is from the bottom of the page to the top.

The puck was dropped using a solenoid release mechanism (see Figure 2.4). In this mechanism the metallic slug holds firmly to the steel backing at 12 Volts. When the applied voltage is turned off, the spring forces the slug back and releases anything being held between the slug and the steel backing. The puck was held by the solenoid through the use of a small tab of aluminum foil. The release angle could then be controlled by changing the attachment point of the slug on the aluminum foil tab.

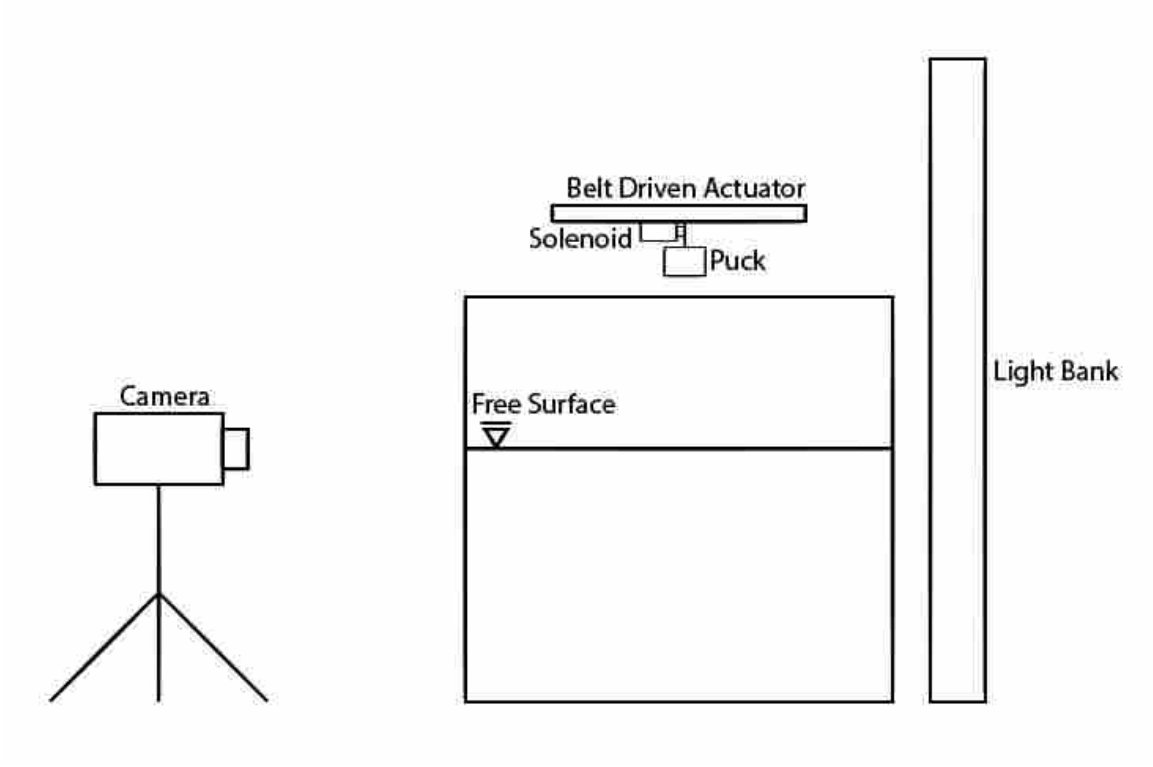

Figure 2.2: A side view of the experimental setup. In this figure the direction of motion is into the page and the camera is filming perpendicular to this plane of motion.

The solenoid drop mechanism was attached to a belt driven actuator to control horizontal velocity (see Fig. 2.5). The entire system was controlled using LabVIEW. The belt was driven by a 3.4 V stepper motor that could reach a maximum of 1.1 m/s. Two photoelectric sensors were used to detect when the drop mechanism had reached the end of the track.

The LabVIEW program was defined in three states. The solenoid drop mechanism was at rest at the beginning of the track in the ”default” state of the LabVIEW program. The solenoid was on holding the puck firmly by the aluminum foil tab. Upon pressing an on-screen start button, the program would switch to a ”running” state and the drop mechanism would accelerate down the track according to a user-defined exponential function. Upon reaching the end of the track, the drop mechanism would cross the photoelectric sensor. Crossing this sensor triggered the program to switch to the ”reset” state. The puck would release, and then the drop mechanism would return to its starting position.

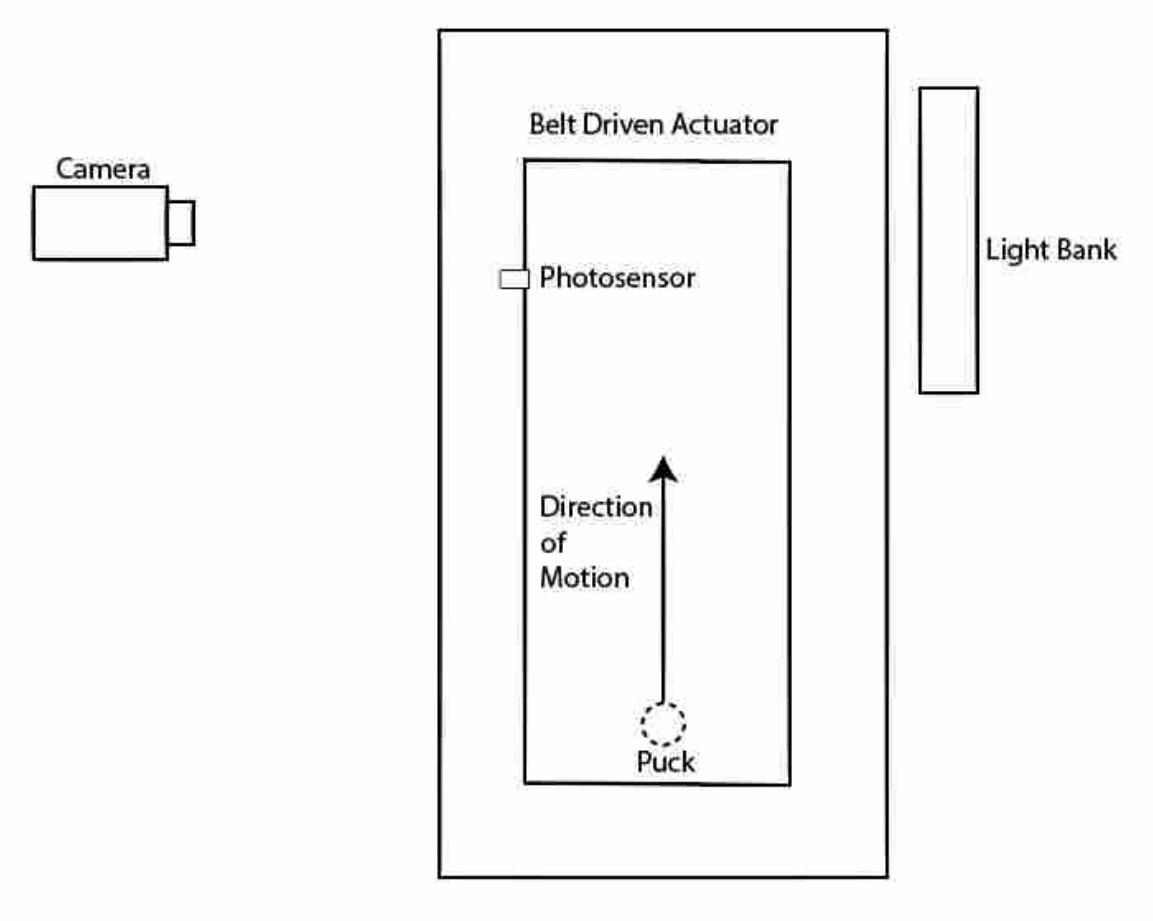

Figure 2.3: A top view of the experimental setup. In this figure the direction of motion is from the bottom of the page to the top and the camera is filming perpendicular to this plane of motion.

The vertical velocity of the puck was controlled by moving the entire apparatus up or down to adjust the drop height. Drag was neglected and the vertical velocity (V_v) was found using:

$$V_v = \sqrt{2gh} \tag{2.1}$$

Neglecting drag was justified by estimating the drag force (F_D) at maximum velocities run in this experiment using $F_D = C_D \rho V^2 A/2$. The force due to gravity was found to be more than an order of magnitude larger than the counteracting force due to drag. A full discussion of the error in vertical velocity can be found in Appendix A.

A second setup was used for additional vertical drop tests. This setup was able to test much higher vertical velocities at the cost of not allowing any horizontal velocity. In this setup the same

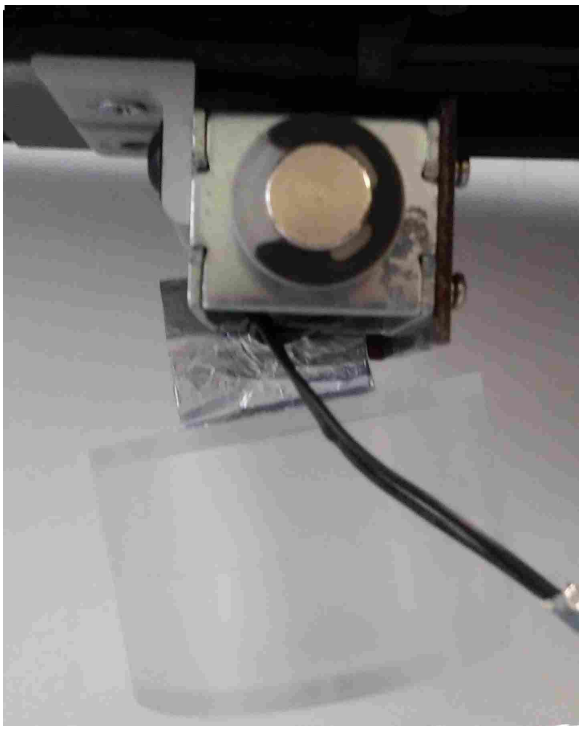

Figure 2.4: Solenoid drop mechanism holding the buoyant cylindrical puck used in this study. The angle of the puck depends upon the attachment point on the aluminum foil tab.

Figure 2.5: Side view of the solenoid drop mechanism attached to a belt driven actuator. The belt was driven by a stepper motor which was controlled using LabVIEW. The aluminum foil tab extending off of the end of the drop mechanism is what the photoelectric sensor detects at the end of the track.

puck was dropped into a 91.4 x 91.4 x 121.9 cm tank of water. The setup was similar to Figure 2.2 except that the solenoid release mechanism was attached in a stationary position over the tank of water. The vertical drop mechanism was able to test vertical velocities of up to 4.85 m/s while the horizontal drop mechanism could only include tests of vertical velocities up to 4.3 m/s.

2.2 Measurement

Measurements were taken from the high-speed images. The horizontal velocity of the puck was calculated to calibrate the motor program settings to velocity. This was done by measuring the horizontal distance the puck traveled in the air while in the frame of the camera. The puck itself was used as a reference to convert pixel distance into meters and time could be calculated using the known frame rate of the camera. All experiments using the same motor settings were averaged together to a single velocity. This method found the horizontal velocity within 0.05 m/s. A discussion of the error in all measurements can be found in Appendix A.

The impact angle (θ) was measured immediately prior to the puck impacting the water by analyzing the high speed images (see Figure 2.6). The pitch angle was also measured and set by hand before the puck started moving in order to fill the experimental field in an efficient manner and reduce the number of repeat tests.

Results from these tests were recorded in terms of a binary (flip/no flip) response. However, in order to more fully understand the trends in the data, cases which did not flip were also given a maximum angle (α) indicating the maximum pitch angle that was reached before returning to a stable upright orientation. The pitch angle could be measured throughout the inversion process and one example of maximum angle is given in Figure 2.7. During preliminary tests this angle was particularly useful in identifying areas in the experimental field which were likely to flip over. A preliminary test in which the puck ”almost flipped over” (defined as a maximum angle greater than 70°) indicated more tests were necessary near that velocity and impact angle. Similarly, a preliminary test which resulted in a low maximum angle indicated tests near that velocity and impact angle were unlikely to flip over.

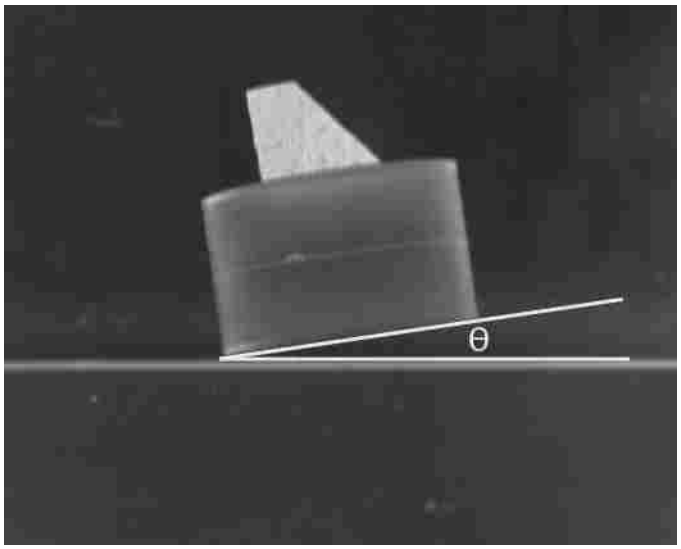

Figure 2.6: The impact angle was measured immediately prior to impact with the free surface. This measurement was taken using an on-screen protractor. The base was placed at the water surface and the measurement was taken along the bottom edge of the puck.

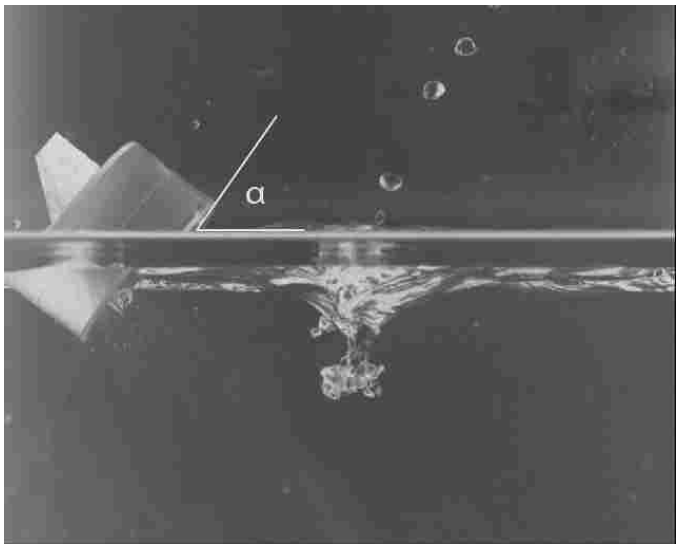

Figure 2.7: Maximum angle (α) of the puck before returning to a stable upright orientation. This measurement was taken using an on-screen protractor. The base was placed at the water surface and the measurement was taken along the bottom edge of the puck.

2.3 Experimental Plan

Several considerations were taken to eliminate experimental error in this experiment. First, A wait time of 10 minutes was imposed between tests to allow the surface waves in the water to settle. After 10 minutes no visual movement at the water surface was noticeable. Surface waves were assumed to be the largest source of error and the residual fluid motion underneath the water was assumed to be negligible. This was further justified by the consistency of the tests. Second, The pitch angle was measured both before release and at water impact. The puck was intended to fall with no angular velocity at impact. If the pitch angle had changed by more than 5° from release to impact, then that test was thrown out. Less than 5 tests were thrown out for this reason. Third, the horizontal velocity was measured after each test to ensure that the program had run as intended.

Four sets of tests were performed in this experiment. A summary of the tests run can be seen in Table 2.1. During preliminary tests, 5 drops were performed at each combination of vertical and horizontal velocity over a wide range of random pitch angles. These tests were intended to fill a large section of the experimental field, identify trends in the data, and identify sections of the experimental field that showed the potential to flip over.

Table 2.1: Range of variables covered in this experiment. A total of 716 tests were performed.

Test Set	Vertical Velocity	Horizontal Velocity	Impact Angle
1	2.5 to 4.8 m/s	0.0 to 1.1 m/s	-10° to 45°
2	3.9 to 4.3 m/s	0.0 to 1.1 m/s	-2° to 25°
3	3.3 m/s	0.0 to 1.1 m/s	-2° to 25°
4	3.65 to 4.85 m/s	0 m/s	0° to 45°

A second set of tests was performed for drop velocities which showed the potential to flip over. During these tests approximately 20 (17-26) tests were performed at each combination of vertical and horizontal velocity. These tests were run to fill the experimental field within 2° for tests which showed the potential to flip over. On multiple occasions a second or third test would land with the same pitch angle, vertical velocity, and horizontal velocity. In these cases, there was never an instance where one flipped over and the other did not.

A third set of tests was performed at a drop height at which preliminary tests indicated no flip would occur. Similar experimental conditions were imposed as the second set. The experimental field was filled within 5° over the range of pitch angles for which the puck was most unstable. This was done to enhance the validity of assumptions made from the first two sets of tests.

Finally, a fourth set of tests was performed using the second setup which allowed only vertical and no horizontal velocity. This set was able to identify trends for much higher vertical velocities. These tests were run to fill the experimental field within 2° in the range of pitch angles which showed the potential to flip over. For vertical drop tests, impacts with a negative pitch angle at impact are reported as positive values. This was done because symmetry makes these cases identical.

CHAPTER 3. RESULTS

3.1 Summary of Results

A total of 716 tests were performed of which 568 data points were collected using the horizontal drop mechanism and 148 data points were collected using the vertical drop mechanism. Of the 716 total tests, 285 inverted upon impact. Vertical velocity, horizontal velocity, and impact angle are all important factors. Increasing vertical velocity increases the likelihood of inversion. Only a limited range of impact angles would flip over at each combination of vertical and horizontal velocity. Inversion is slightly more common at higher horizontal velocities. However, the larger effect of increasing the horizontal velocity was to shift the range of θ for which the puck will flip to lower angles. General trends established will be discussed in depth throughout the rest of this chapter.

3.2 The Inversion Process

The mechanism of inversion can be seen by examining the high-speed video recorded in this experiment. Each video was recorded such that the direction of the horizontal velocity was right to left in the plane of the camera. The puck flipped in a counter-clockwise direction. Each test conducted in this experiment followed the same general pattern. This process can be seen in Figure 3.1. The puck does not directly flip over with a continuous angular momentum as can be seen clearly in the graphs of angle and angular velocity plotted over time in Figure 3.2. Rather, at water impact an asymmetrical cavity forms on the back side of the puck. The puck falls into the cavity. At this point the puck is actually rotating in a clockwise direction. Then, as the cavity collapses, a jet is formed which impinges on the side of the puck and a moment is applied to the puck which ultimately flips it over in the counter-clockwise direction.

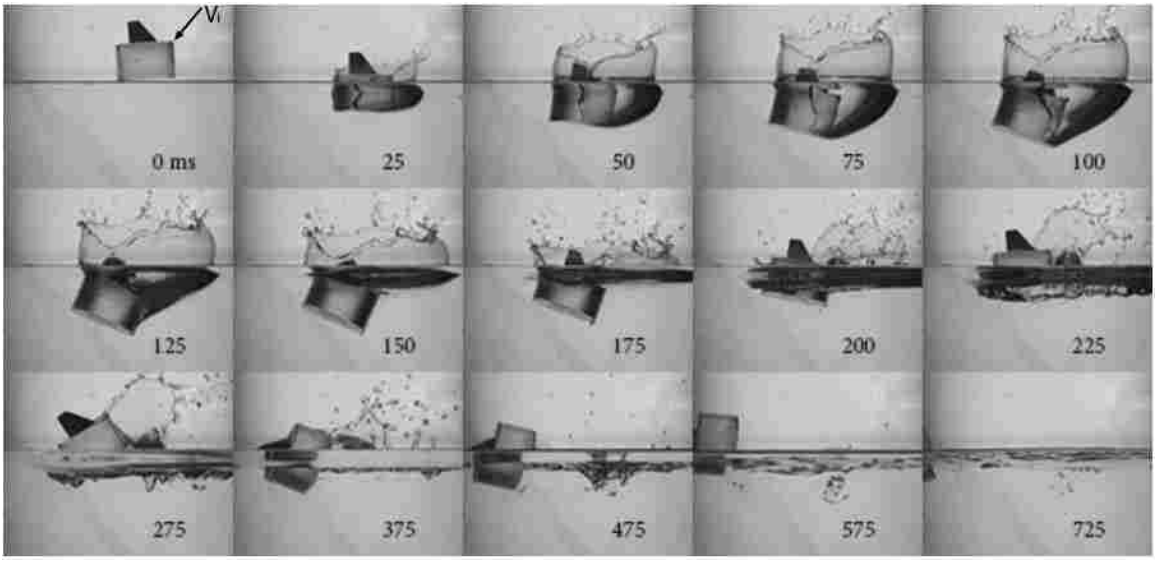

Figure 3.1: Inversion sequence for a buoyant cylindrical puck drop with V_v=3.9 m/s, V_h=1.1 m/s, and θ=3°. An asymmetrical cavity forms around the puck (25-100 ms). As the cavity collapses, (125-175 ms) a line of water remains attached to the puck and applies a moment which flips it over. At 725 ms the puck begins to leave the frame, but is clearly at a point where it will continue to fall to an inverted orientation.

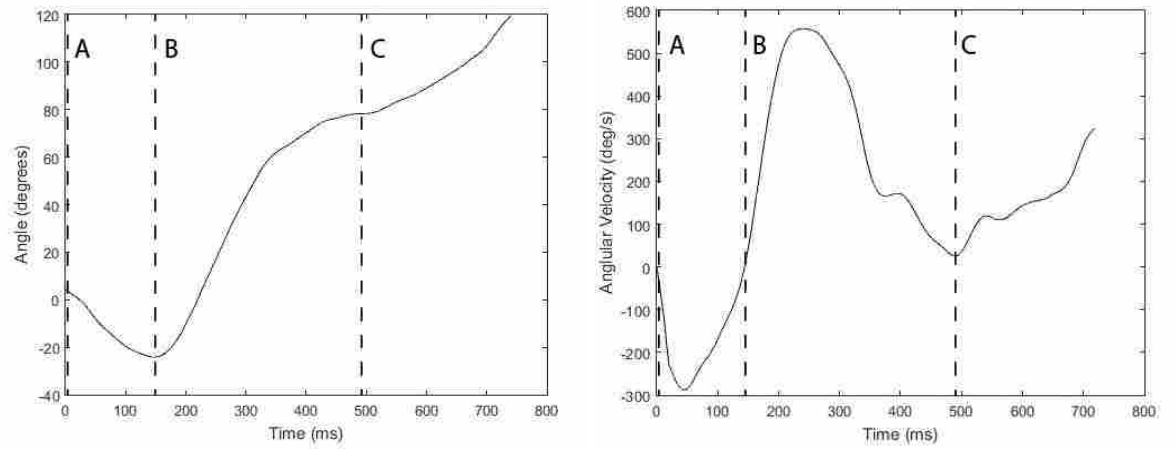

(a) (b)

Figure 3.2: Pitch angle (a) and angular velocity (b) plotted over time for the inversion sequence in Figure 3.1 (V_v=3.9 m/s, V_h=1.1 m/s, and θ=3°.) The initial impact (A), cavity collapse (B), and a local minimum in angular velocity (C) are marked by dashed lines. During the initial impact (0-150 ms) the puck sits back into the cavity with a negative angular velocity. After cavity collapse (150 ms) a strong angular velocity develops in the opposite direction nearing a maximum of 600 deg/s. The angular velocity decreases to near 0 as the puck nears its 90° stability point. This moment is marked by C. After passing this stability point the angular velocity again increases as it falls to an inverted orientation.

The angular velocity graph presented in Figure 3.2 is comparable to angular velocity data obtained by Lorenz for the TiME capsule (see Figure 3.3). The same pattern of an initial negative angular velocity followed by a strong positive angular acceleration upon cavity collapse is seen. In both cases gravity nearly stops the angular acceleration, but it continues to fall as it has already passed its midway stability point.

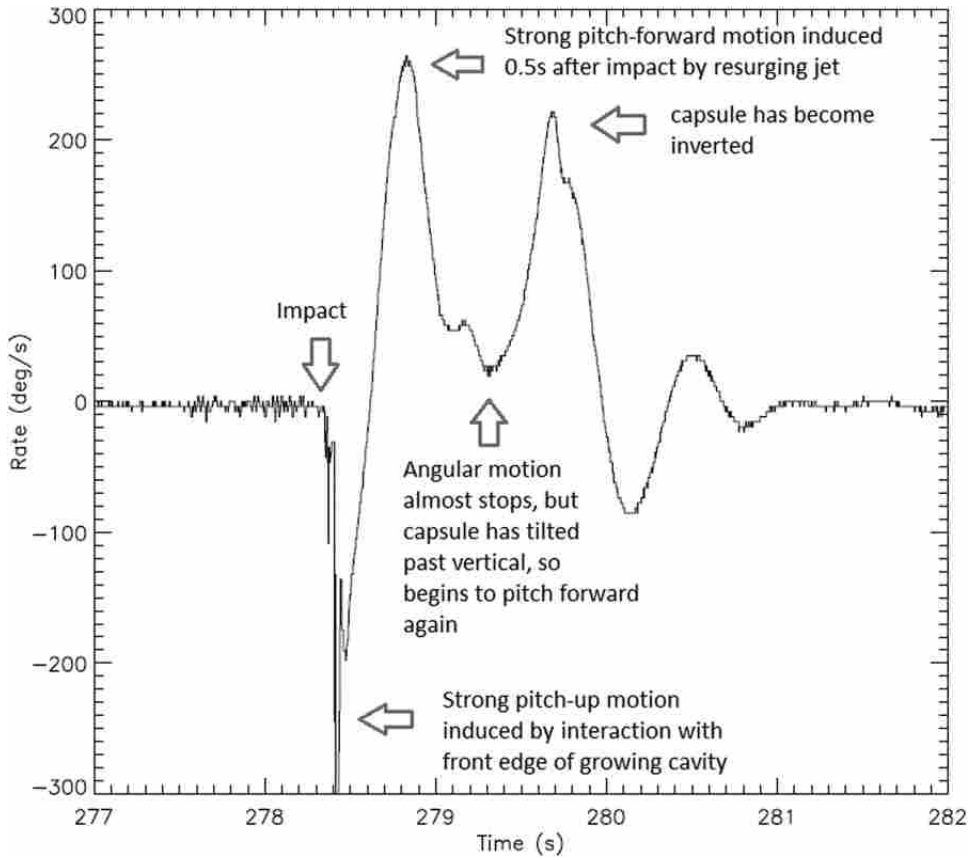

Figure 3.3: Angular velocity plotted over time for the TiME capsule [26]. Similar to the cylindrical puck, the capsule undergoes an initial negative angular acceleration, followed by a strong positive angular acceleration upon cavity collapse. This graph follows the pitch angle for a longer period of time compared to Figure 3.2. This explains the additional peaks found in this graph.

The cause of angular velocity changing directions becomes clear by examining force diagrams at three important moments in the inversion process. Figure 3.4 shows forces acting on the puck just after water impact. This corresponds to a time between 0 and 25ms in Figure 3.1. During this time the puck rotates with a negative angular velocity. The drag force (F_D) acts in the opposite direction to the velocity vector (V) and applies an immediate moment upon water impact.

Added mass (M_A) is also approximated acting in the opposite direction to the velocity vector at the centroid of the submerged area. Drag force and added mass could be combined by integrating pressure over the submerged surface area.

The relative magnitude and direction of the moment applied due to these forces depends upon the horizontal velocity and the pitch angle at impact. An extremely high horizontal velocity and impact angle can result in immediate ”tripping” caused by the horizontal component of this force. A hydrostatic force (F_H) also applies a moment and acts primarily on the leading side of the puck. The gravitational force (F_G) acts through the center of gravity (C_G) and applies no moment.

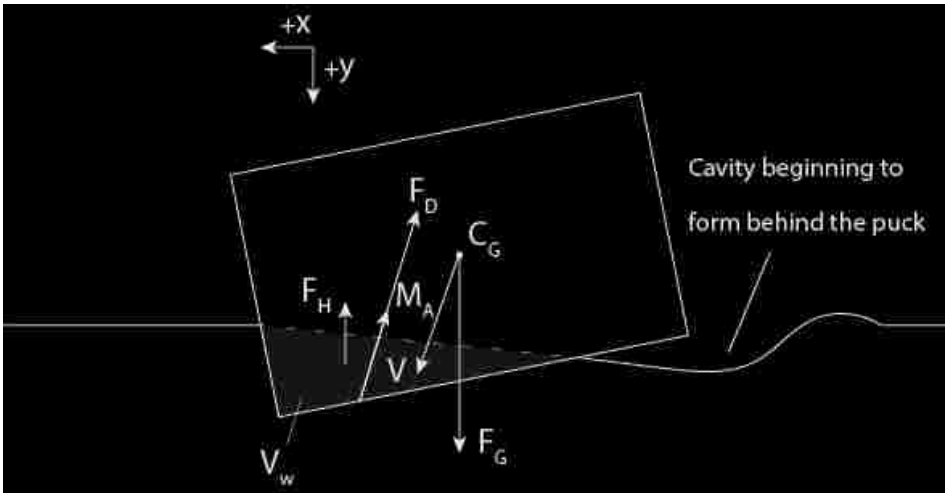

Figure 3.4: Forces acting on the puck just after water impact. This corresponds to a time between 0 and 25ms in Figure 3.1. V is the velocity vector, V_W is the wetted area of the puck, F_D is the drag force, M_A is the added mass, F_H is the hydrostatic force, and F_G is the force due to gravity. The moments applied at this time cause the puck to rotate into the cavity. These force vectors are not necessarily drawn to scale.

At 150ms in Figure 3.1 the puck has reached its minimum angle and the angular velocity has gone to zero. The forces acting at this time are shown in Figure 3.5. The relative importance of drag force has diminished because the velocity has decreased to near zero. However, a hydrostatic force is still applying a moment. This force acts through the center of buoyancy which constantly changes with both the wetted area and depth of the puck in the water. Added mass is also still present because the puck is accelerating. In this instant the cavity has almost entirely collapsed.

However, the jet has not yet impinged on the side of the puck and the resulting moment has not yet been applied.

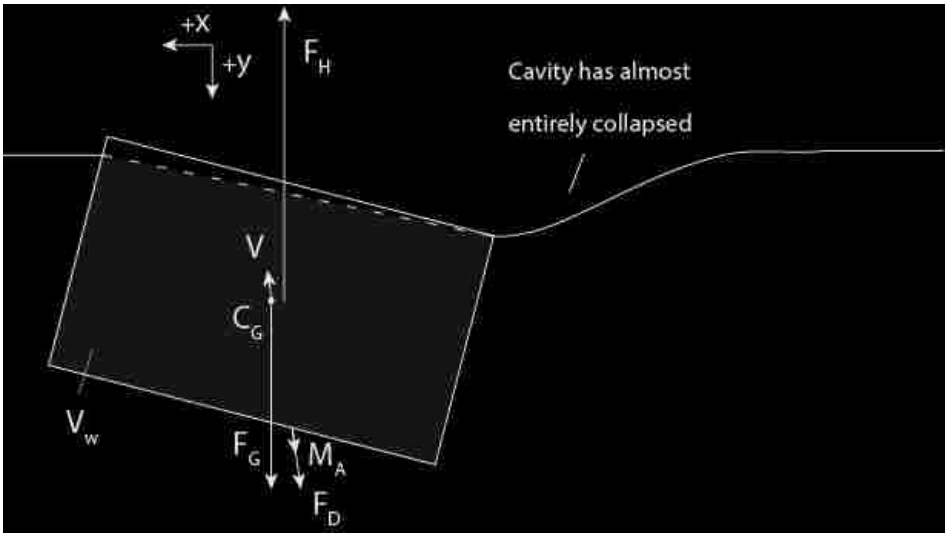

Figure 3.5: Forces acting on the puck when the angular velocity is at zero. This corresponds to a time of 150ms in Figure 3.1. V is the velocity vector, V_W is the wetted area of the puck, F_D is the drag force, M_A is the added mass, F_H is the hydrostatic force, and F_G is the force due to gravity. The cavity has almost entirely collapsed but the jet has not jet impinged on the side of the puck.

Figure 3.6 shows the forces acting on the puck upon cavity collapse. A large force (F_J) is applied as a jet impinges on the side of the puck. This force lifts the puck out of the water and applies a moment which ultimately flips it over. A hydrostatic force is still acting on the puck, but the relative importance of this force has diminished as the majority of the puck has lifted above the water surface. After jet impingement the jet fans out in the plane of motion.

3.3 The Effect of Vertical Velocity on Inversion

The same general process is seen in when the puck is dropped with lower vertical velocity (see Figure 3.7). In Figures 3.1 and 3.7 the puck was dropped with a horizontal velocity of 1.1 m/s and an impact angle of 3°. The only difference is that the puck in Figure 3.7 was dropped with 0.6 m/s less vertical velocity. When the puck impacted the water with a lower vertical velocity, less energy was transferred to the resulting cavity. This resulted in less energy transferred back to the puck in the form of angular momentum when that cavity collapsed.

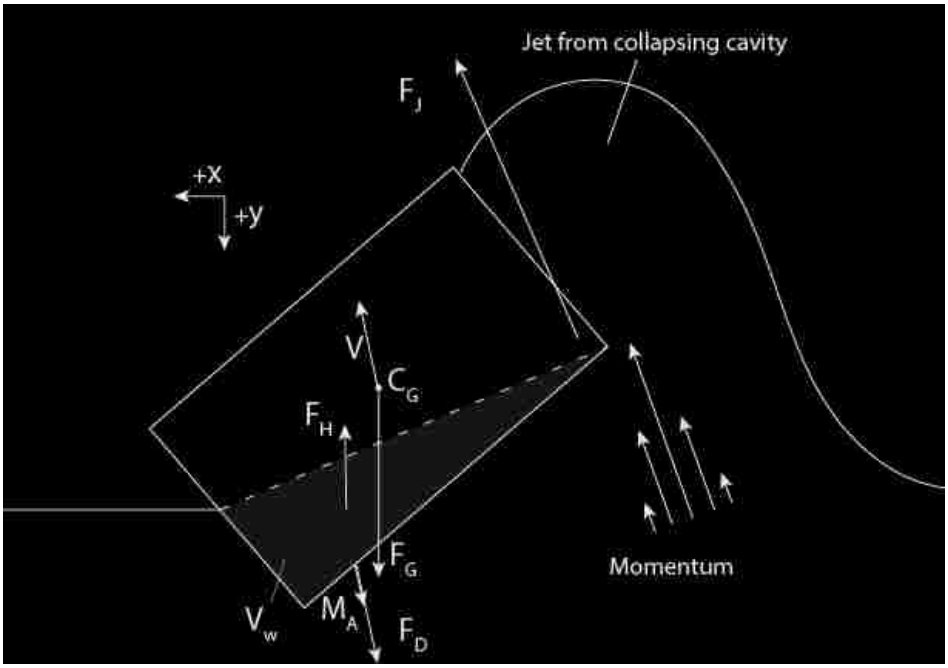

Figure 3.6: Forces acting on the puck upon cavity collapse. This corresponds to a time between 200ms and 275ms in Figure 3.1. F_H is the hydrostatic force and F_G is the force due to gravity. A jet impinges upon the side of the puck and applies a large force (F_J). This force applies a moment which ultimately flips the puck over. The vertical component of F_J is large enough to lift the majority of the puck out of the water. Added mass (M_A) and drag (F_D) are again acting in the opposite direction to the velocity vector.

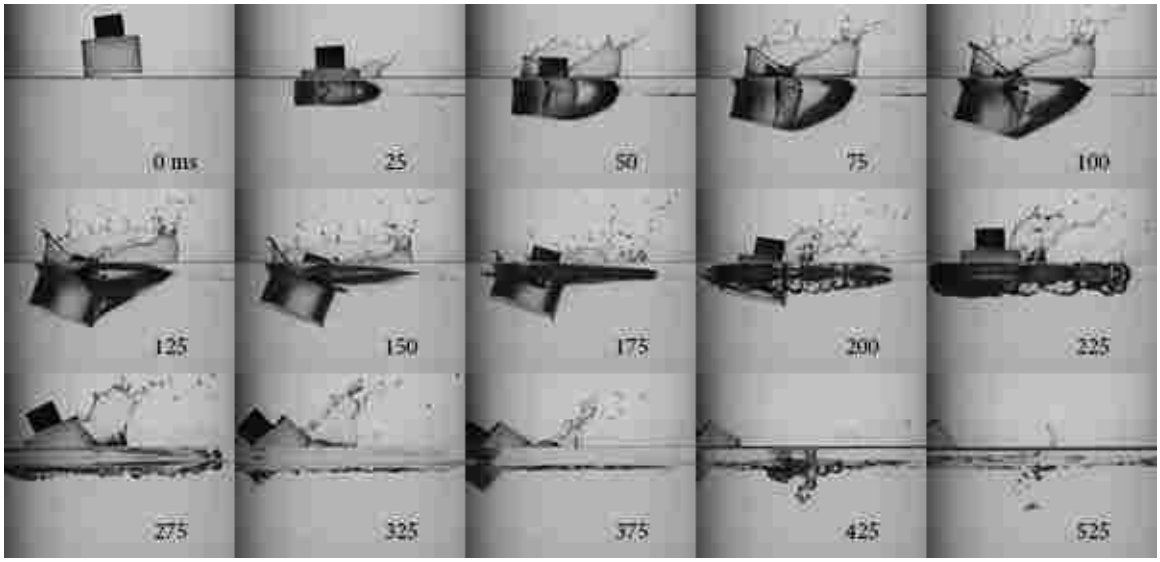

Figure 3.7: Image sequence for a buoyant cylindrical puck drop with V_v=3.3 m/s, V_h=1.1 m/s, θ=3°. A similar process occurs as in the higher vertical velocity case. However, a significantly smaller moment is applied. This results in the puck falling back to an upright orientation.

While the general process of these two cases is quite similar, an inspection of the individual frames reveals two important differences. First, the splash curtain is significantly larger for the higher velocity case. The splash curtain does not cause the puck to flip, but rather is clear evidence of the larger energy stored in the cavity of an impact with higher vertical velocity. Second, the puck sits deeper in the water in the higher velocity case. At 125 ms, when the cavity begins to collapse, the top of the puck in the higher velocity case is seen well below the water surface. In the lower velocity case the top of the puck appears to be just at the water surface. The decreased energy in the cavity of the lower velocity case is insufficient to flip the puck over.

As is noted by Lorenz [3] a critical vertical velocity exists below which the puck would never flip over. During vertical drop tests, no puck flipped with a vertical velocity at or below 3.9 m/s (see Figure 3.8). When a horizontal velocity was added, pucks flipped over at a vertical velocity of 3.9 m/s; however, no puck flipped over at a vertical velocity of 3.75 m/s. It appears that this can be entirely accounted for by distinguishing between the vertical velocity and the total impact velocity as defined by: $V_i = \sqrt{V_h^2 + V_v^2}$. The range of impact angles for which the puck would flip over grows wider as the vertical velocity increases. This range increases asymmetrically. As vertical velocity increases the range of angles for which the puck will flip over grows far more quickly with larger angles than for smaller angles. At $V_v = 4.1$ m/s the range of angles for which the puck will flip is centered at 14.5°. At the highest vertical velocity tested ($V_v = 4.85 m/s$) the range is centered at 17°.

A summary of all drop tests using the horizontal drop mechanism can be seen in Figure 3.9. It should be noted in this graph that all tests which flipped over are bounded by a 3-dimensional shape. All tests which fell in this region flipped over. On this 3-dimensional shape there is no lower or upper bound on horizontal velocity and there is also no upper bound on vertical velocity. However no test flipped over below a vertical velocity of 3.75 m/s. A clearer view of the bounds on this graph will become evident by examining cross-sections.

A similar pattern was seen in the Apollo missions [4]. Two vertical velocities were tested most extensively during the testing phase. If all three parachutes deployed as expected the command module would fall with a terminal velocity of 8.5 m/s. However, if only two parachutes deployed, the terminal velocity increased to 10.3 m/s. It was found during these tests that inversion was much more likely at the higher impact velocity.

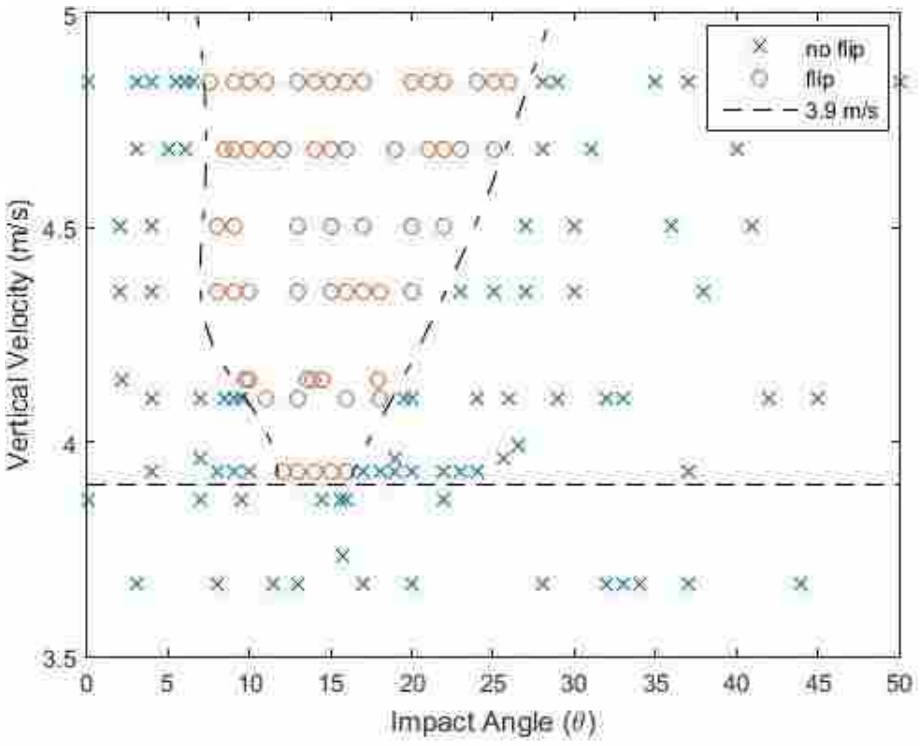

Figure 3.8: A summary of all tests completed using the vertical drop mechanism. The range of θ for which the puck will flip over upon impact tended to increase with an increasing V_v. Error in vertical velocity is estimated at plus or minus 0.05 m/s and error in impact angle is estimated at plus or minus 0.5°. A full discussion of error can be found in Appendix A.

3.4 The Effect of Pitch Angle at Impact on Inversion

Each combination of V_h and V_v for which the puck had the potential to flip over would only do so over a specific range of θ. If θ was either too high or too low the puck would not invert. Figure 3.10 gives an example of an image sequence for a puck which did not flip over because θ was too high. This image sequence has the same values for V_v and V_h as Figure 3.1.

In the high pitch angle case a larger splash curtain forms in front of the puck than behind it. The effect of this can be seen at 125 ms. The high pitch angle case sits back into the cavity at a shallower angle compared to the lower pitch angle case. When the puck does not sit back into the cavity, a much smaller moment is applied during cavity collapse.

Greater intuition as to why this is the case can be gained by examining vertical drop cases at extreme angles. Figures 3.11 - 3.13 show three cases of a vertical drop 50 ms after impact. A typical impact which did ultimately invert is shown in figure 3.11. The cavity and splash curtain are

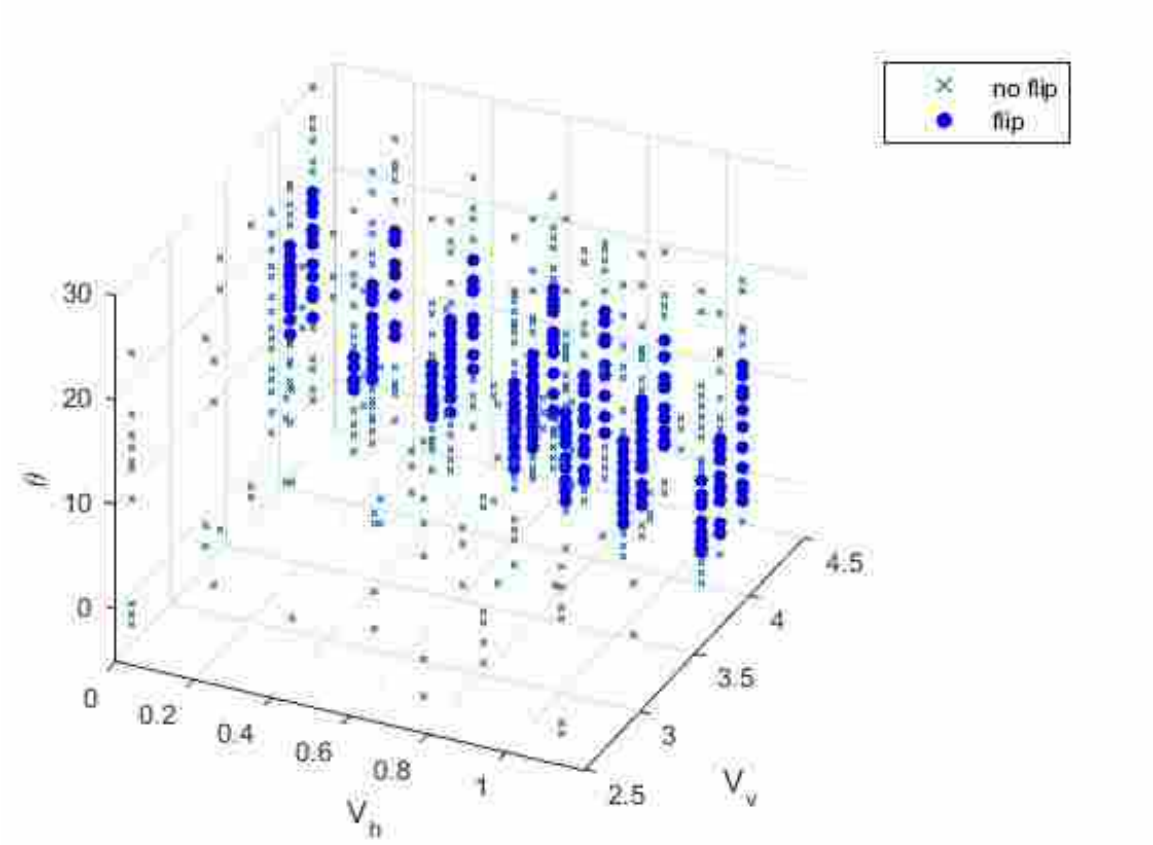

Figure 3.9: A summary of all data collected using the horizontal drop mechanism. Out of 568 tests 223 inverted upon impact. No tests inverted below $V_v = 3.75m/s$. Some tests flipped over in every value of V_h that was tested. All tests that inverted are clumped together and no test which did not invert falls in this region.

both asymmetrical and focused behind the puck. This puck has already begun to sit back into the open cavity. Figure 3.12 shows an impact with $\theta = 0°$. The cavity and resulting splash curtain are symmetrical and cannot apply a moment to the puck upon collapse. Figure 3.13 shows an impact with an extremely high angle ($\theta = 41°$). While the impact of a cylinder is not symmetrical at this angle, you can begin to see the splash curtain being pushed to both the left and right of the puck. The impact does not allow the puck to sit back in the water, and as a result, very little moment is applied to the puck upon cavity collapse.

For cases which did not invert upon impact, a maximum angle (α) was measured indicating the closest angle to flipping over that the puck reached before returning to an upright orientation. This was done to clearly identify areas which were close to flipping over. Figure 3.14 shows

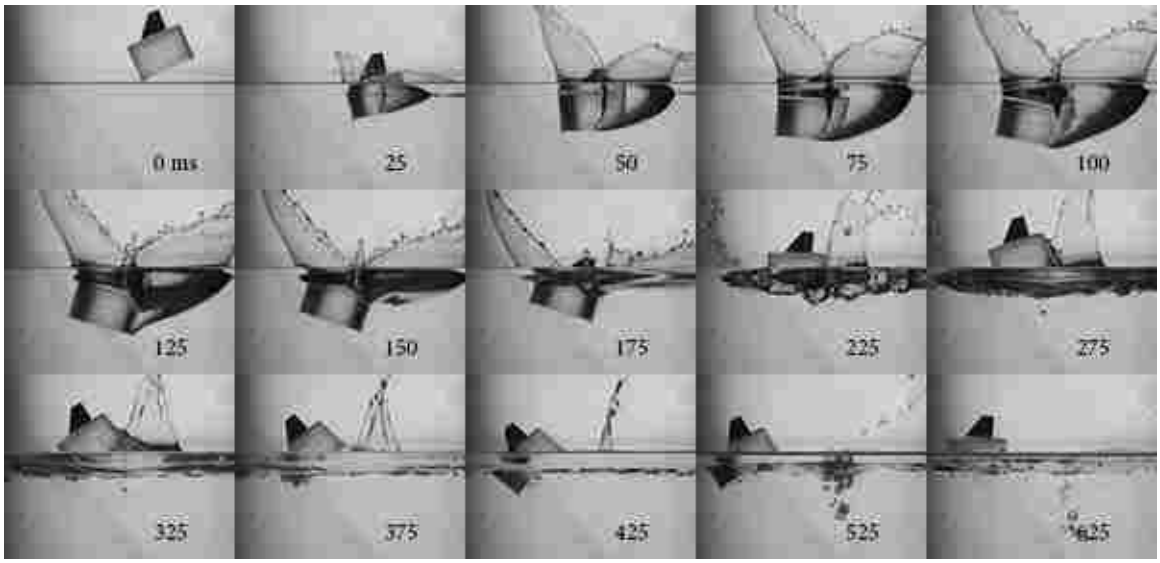

Figure 3.10: Image sequence for a buoyant cylindrical puck drop with V_v=3.9 m/s, V_h=1.1 m/s, θ=24°. At a higher pitch angle at impact the majority of the splash curtain is pushed in front of the puck. The puck does not sit back into the cavity as deeply and a smaller moment is applied upon cavity collapse.

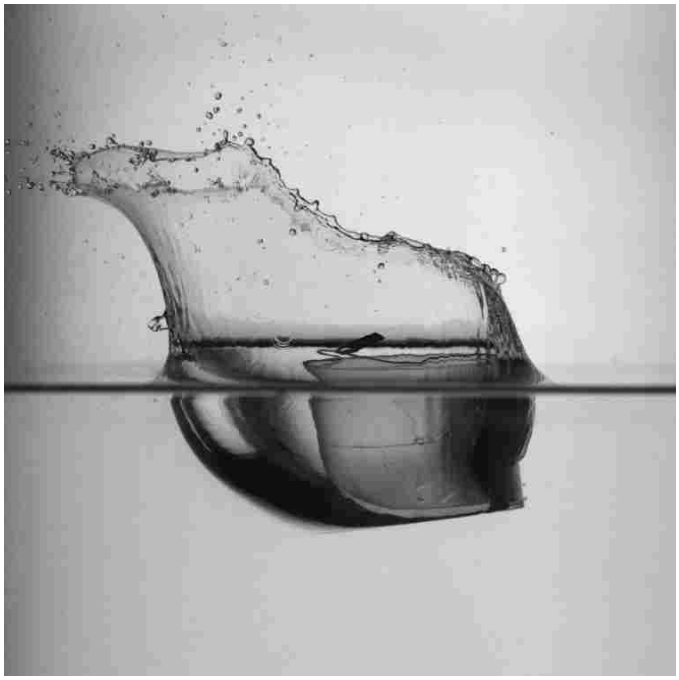

Figure 3.11: A vertical drop case 50 ms after impact for θ=8°. An asymmetrical cavity is forming behind the puck and the puck is beginning to sit back into this cavity. Upon cavity collapse this test case flipped over.

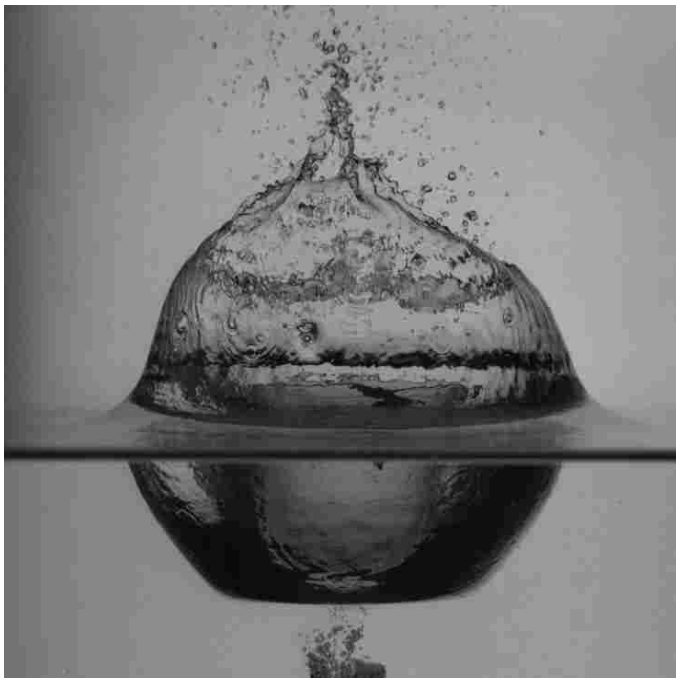

Figure 3.12: A vertical drop case 50 ms after impact for θ=0°. A symmetrical cavity is forming around the puck. Upon cavity collapse the puck experiences an equal force on both sides and simply raises up with no moment applied.

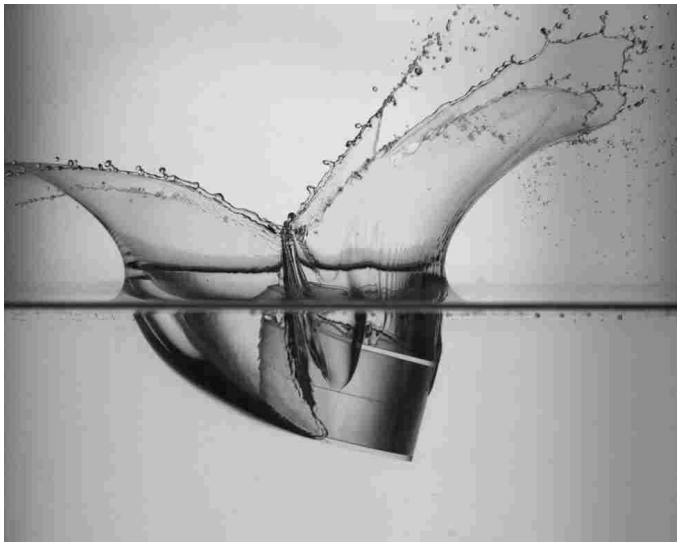

Figure 3.13: A vertical drop case 50 ms after impact for θ=41°. At this high impact angle the puck dives into the water. The puck does not sit back into the cavity as is seen in previous cases. When the cavity collapses, an insignificant moment is applied and the puck remains stable and upright.

α mapped over a range of velocities which never flipped over. The same general shape is seen between the three horizontal velocities shown in this figure. For each V_h there is an impact angle for which the puck is closest to flipping over. To the left or right of these maxima α tends to decrease. As vertical velocity increases this same general shape would be seen; however, all cases with a maximum angle over 80 degrees ended up flipping over.

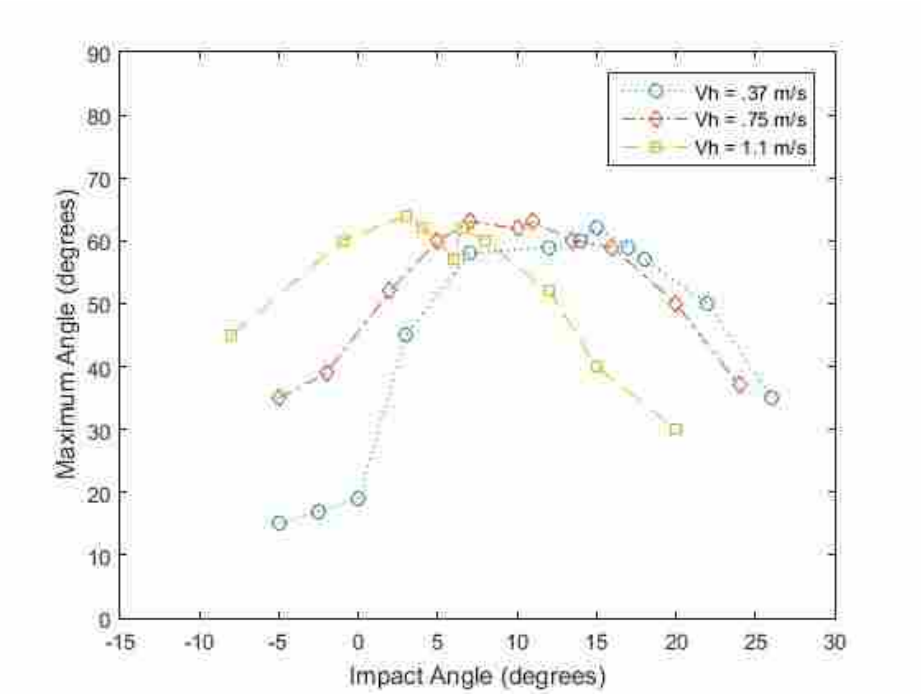

Figure 3.14: The maximum angle reached before returning to a stable upright orientation is plotted at three horizontal velocities for V_v=3.3 m/s. The same general shape is seen for each horizontal velocity. The graph shifts to the left along the x-axis as horizontal velocity increases. Error in horizontal velocity is estimated at plus or minus 0.05 m/s and error in impact angle is estimated at plus or minus 0.5°. A full discussion of error can be found in Appendix A.

3.5 The Effect of Horizontal Velocity on Inversion

The largest difference between the three different horizontal velocities shown in Figure 3.14 is a horizontal shift. The pucks with a higher horizontal velocity were not significantly less stable overall; however, the angles for which they were unstable were shifted to the left. This result is further supported by video evidence and the data for horizontal drop tests. Figures 3.15 and 3.16

show two tests run under the same vertical velocity and impact angle with different horizontal velocities. In this instance the test case with the higher horizontal velocity is more stable while the lower horizontal velocity inverts upon impact. However, at lower impact angles the puck was more stable at lower horizontal velocities.

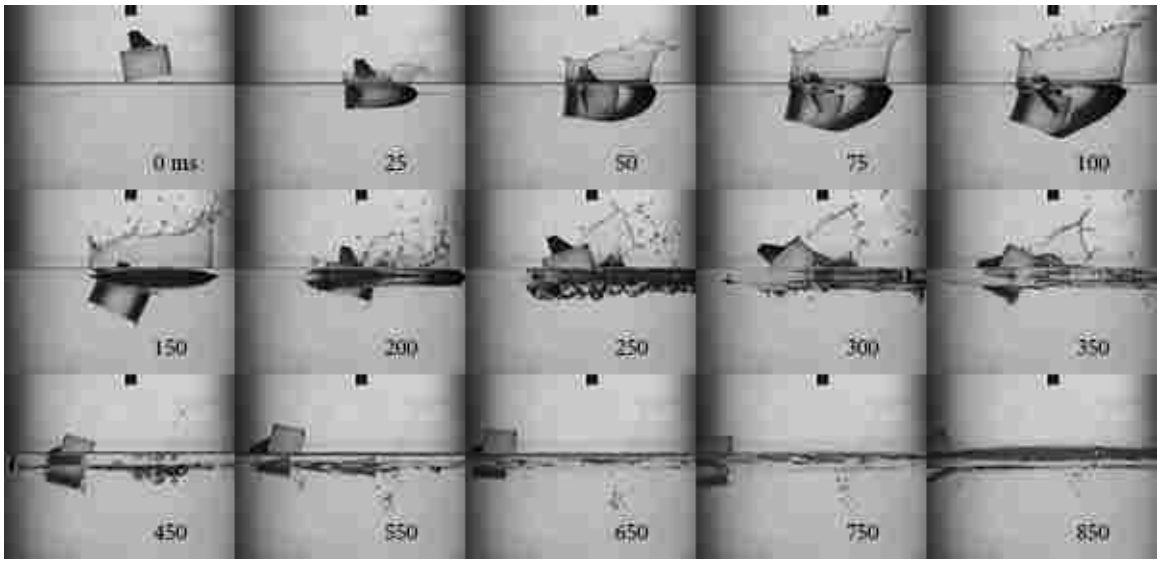

Figure 3.15: Inversion sequence for a buoyant cylindrical puck with V_v=3.9 m/s, V_h=0.6 m/s, and θ=8°. An asymmetrical cavity forms around the puck (25-100 ms). As the cavity collapses, (150 ms) a line of water remains attached to the puck and applies a moment which flips it over.

Only minor differences occur between the two cases presented in Figures 3.15 and 3.16. At 100 ms each puck is in an almost identical position. The puck is sitting back in the cavity as the cavity is about to collapse. However, the splash curtain is slightly higher in front of the high horizontal velocity case. Ultimately, a slightly stronger moment is applied on the lower horizontal velocity case which flips it over.

Three drop heights were tested with the horizontal drop mechanism for which the puck had the potential to flip over. These results are shown in Figures 3.17 - 3.19. Several lower drop heights were tested in which inversion was never seen. The trend seen previously is reinforced with higher V_h causing the impact angles for which the puck is unstable to shift to the left.

The results for Figure 3.19 shows results for the one case in which increasing V_h significantly widened the range of θ for which the puck inverts upon impact. In this case, the vertical

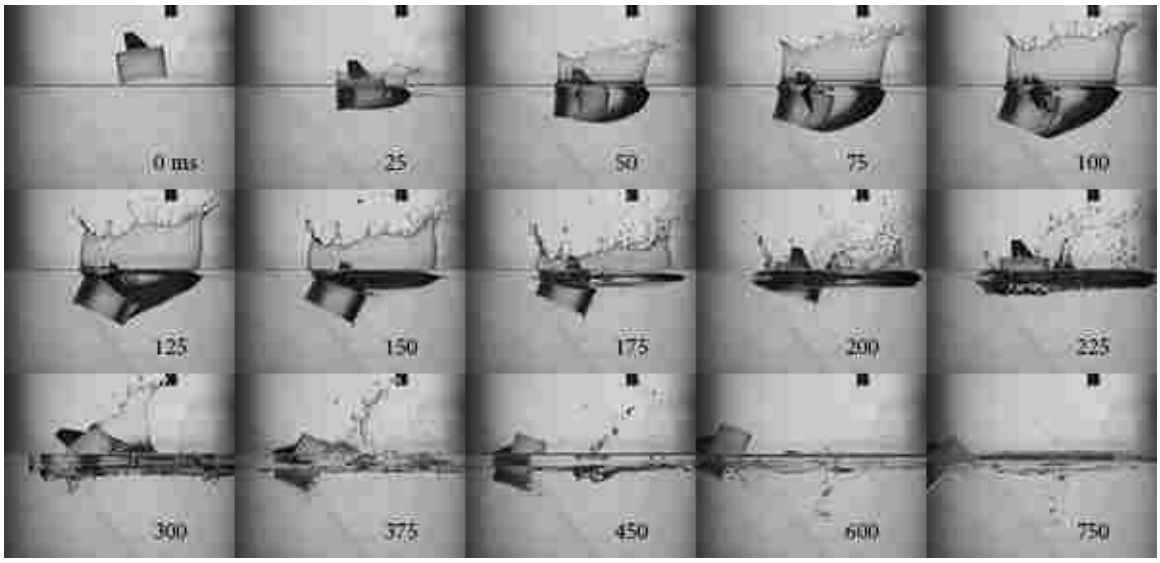

Figure 3.16: Inversion sequence for a buoyant cylindrical puck with V_v=3.9 m/s, V_h=1.1 m/s, and θ=8°. A very similar process occurs as is seen in the lower horizontal velocity case. However, in this case, a slightly higher splash curtain can be seen in front of the puck. As the cavity collapses, the applied moment does not flip the puck over.

velocity is close to the minimum impact velocity for which the puck will flip over. The total impact velocity as defined by: $V_i = \sqrt{V_h^2 + V_v^2}$ increases through the critical range for which the puck begins to flip over. Horizontal velocities above 0.6 m/s show a clear trend shifting unstable pitch angles at impact to the left as horizontal velocity increases.

A similar trend is seen at a vertical velocity of 4.1 m/s. However, in this case the range of angles for which the puck will invert is almost identical throughout the entire range of horizontal velocities. At $V_h = 0$ m/s the range of angles for which the puck will flip over is 8.5°. At $V_h = 1.1$ m/s the range of angles for which the puck will flip over is 9° wide. This range is measured within 2° accounting for the error in measurement and the resolution of the tests. However, the center of those ranges shifts significantly to the left, moving from 13° to 3.5°.

A wider range of angles flip over at a vertical velocity of 4.3 m/s as seen in figure 3.19. At $V_h = 0$ m/s the range of angles for which the puck will flip over is 12° wide. At $V_h = 1.1$ m/s the range of angles for which the puck will flip over is 13° wide. The difference between these ranges is within the error level of the tests. The same general trend is seen as in lower vertical velocities. The pitch angles for which the puck is unstable shifts to the left as horizontal velocity increases.

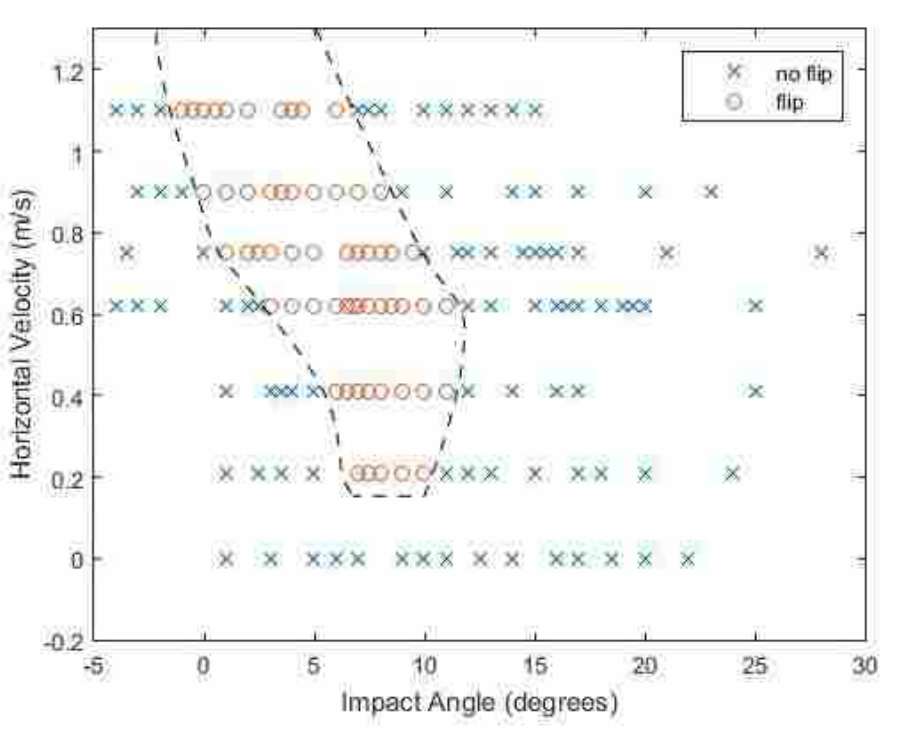

Figure 3.17: Inversion data for V_v=3.9 m/s. No cases flipped over for tests with $V_h = 0$. The range of angles for which the puck would flip over widened until $V_h = 0.6$ m/s. As horizontal velocity increased the range of angles for which the puck would flip over shifted to the left. Error in horizontal velocity is estimated at plus or minus .05 m/s and error in impact angle is estimated at plus or minus 0.5°. A full discussion of error can be found in Appendix A.

3.6 Condensing the Data

An asymmetrical cavity could form through either introducing a horizontal velocity or a pitch angle at impact. Increasing the horizontal velocity had the same effect as increasing the pitch angle at impact. This suggests the possibility of collapsing this data by combining these two variables into one term. This was done by defining a trajectory angle (β) as seen in Figure 3.20 and introducing a new variable for adjusted impact angle (ϕ) defined by Equation 3.1. In this equation θ is the impact angle and ζ is a coefficient describing the relative importance of trajectory angle obtained from experimental testing.

$$\phi = \theta + \zeta\beta \tag{3.1}$$

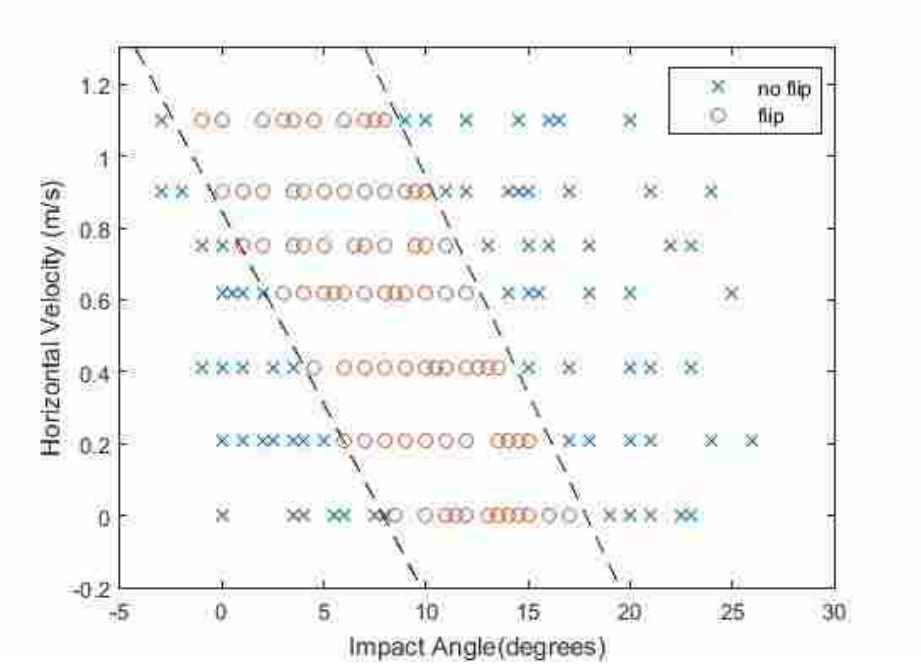

Figure 3.18: Inversion data for V_v=4.1 m/s. Cases flipped over for all values of V_h that were tested. The width of the range of angles for which the puck would flip over remained fairly constant across all values of V_h. As horizontal velocity increased the range of angles for which the puck would flip over shifted to the left. Error in horizontal velocity is estimated at plus or minus .05 m/s and error in impact angle is estimated at plus or minus 0.5°. A full discussion of error can be found in Appendix A.

This method proved to be most effective at higher vertical velocities as is seen in Figures 3.21 and 3.22. In these figures it can be seen that the section of data that will flip over can very nearly be described perfectly using two vertical lines with the range between these lines being larger for the higher vertical velocity case. However, the coefficient ζ used increases slightly from 0.55 in the 4.3 m/s case to 0.6 in the 4.1 m/s case.

For a vertical velocity of 3.9 m/s (see Figure 3.23the data is a little unclear because the range of angles for which the puck would flip tapers off at lower horizontal velocities. However, the data still condenses significantly between two vertical lines. This same effect is seen with a maximum angle graph at a vertical velocity (3.9 m/s) which never flipped over. The graphs come close together, but do not collapse perfectly onto one shape. The coefficient (ζ) continues to increase as vertical velocity decreases. For a vertical velocity of 3.9 m/s $\zeta = .63$ and for a vertical velocity of 3.3 m/s $\zeta = .65$.

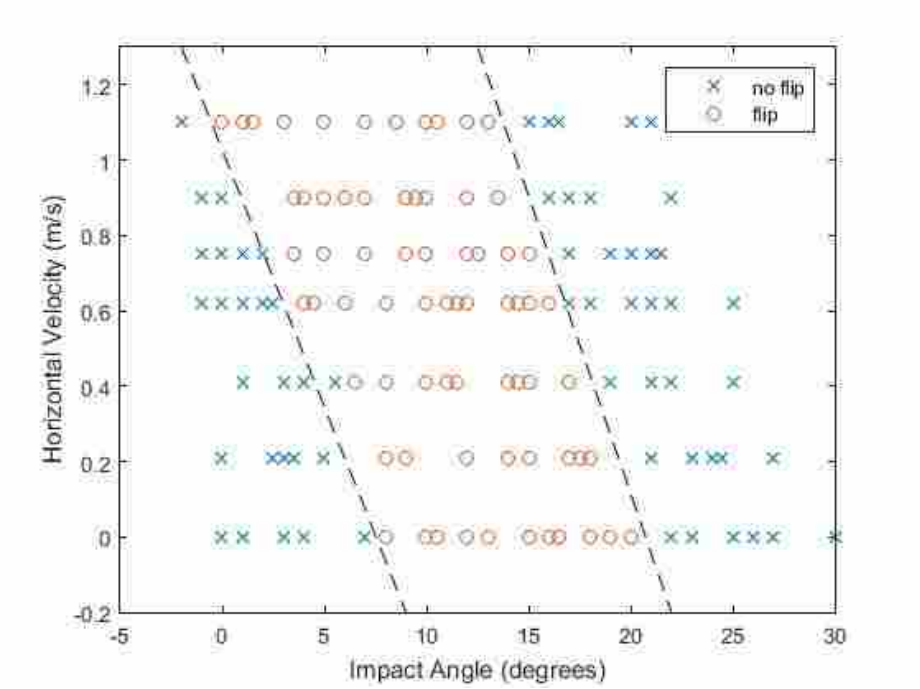

Figure 3.19: Inversion data for V_v=4.3 m/s. Cases flipped over for all values of V_h that were tested. The width of the range of angles for which the puck would flip over remained fairly constant across all values of V_h. As horizontal velocity increased the range of angles for which the puck would flip over shifted to the left. Error in horizontal velocity is estimated at plus or minus .05 m/s and error in impact angle is estimated at plus or minus 0.5°. A full discussion of error can be found in Appendix A.

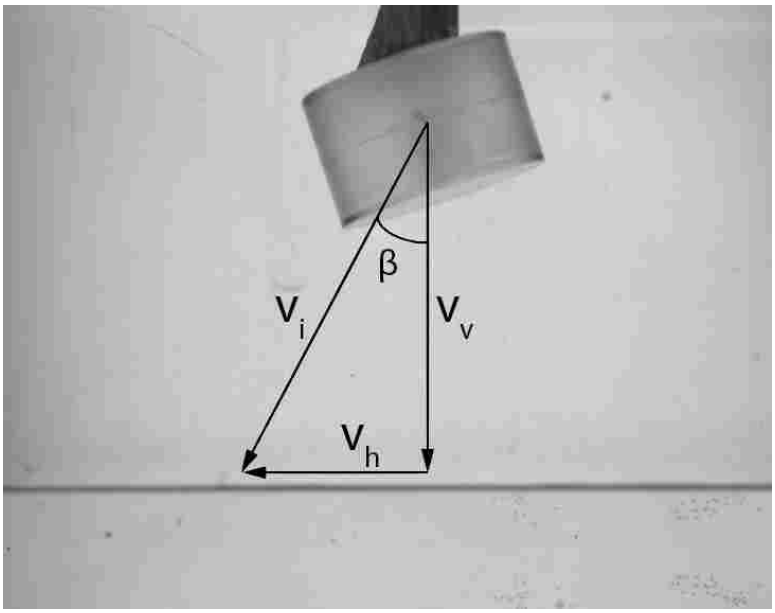

Figure 3.20: The trajectory angle β was calculated using the horizontal and vertical velocities

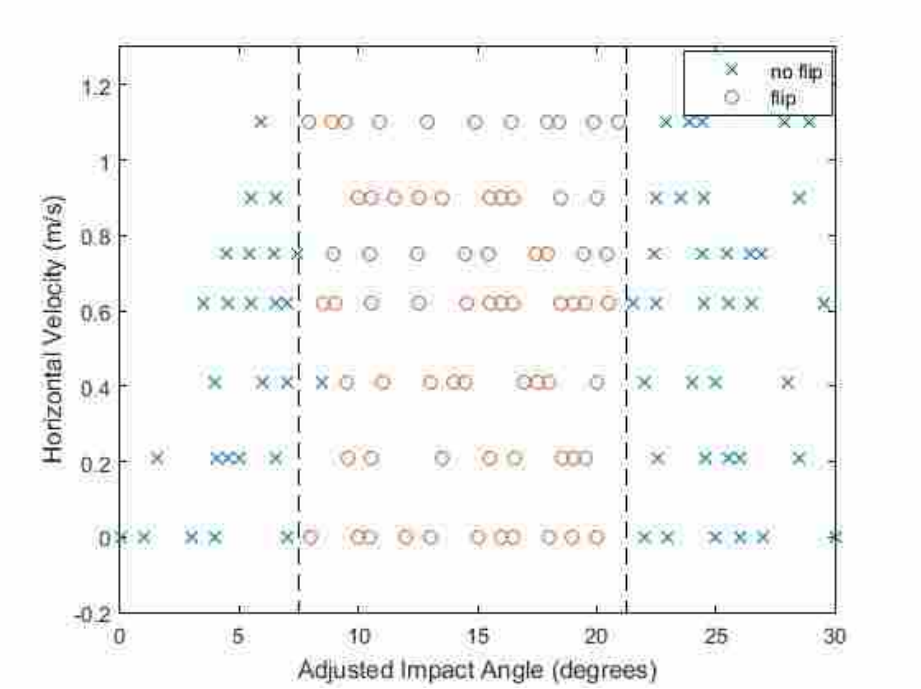

Figure 3.21: Adjusted inversion data for V_v=4.3 m/s using an adjusted impact angle (ϕ) which incorporates the trajectory angle. In this case $\zeta = 0.55$. Almost all of the flip data is defined by two vertical lines.

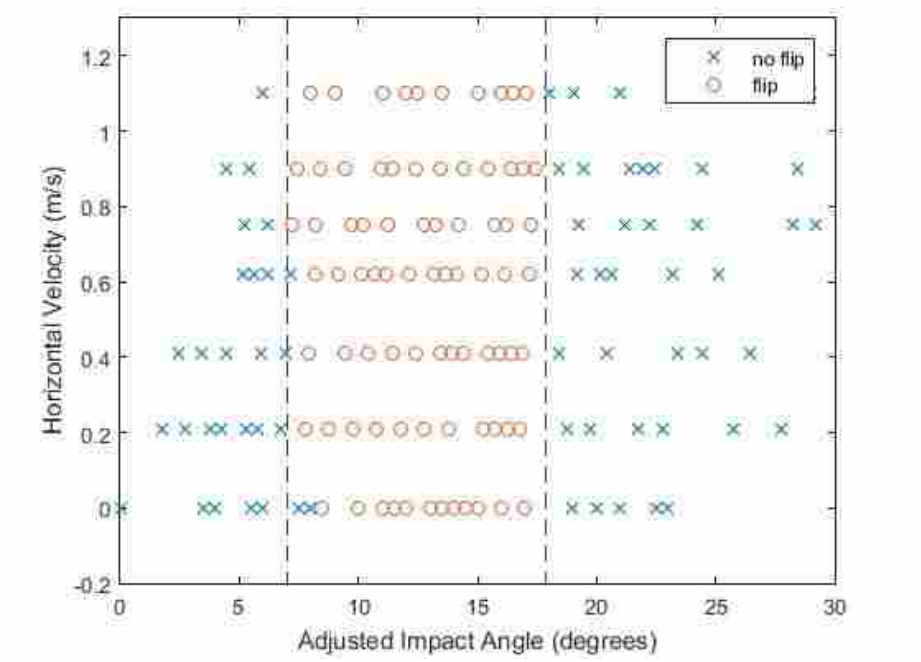

Figure 3.22: Adjusted inversion data for V_v=4.1 m/s using an adjusted impact angle (ϕ) which incorporates the trajectory angle. In this case $\zeta = 0.6$. Almost all of the flip data is defined by two vertical lines.

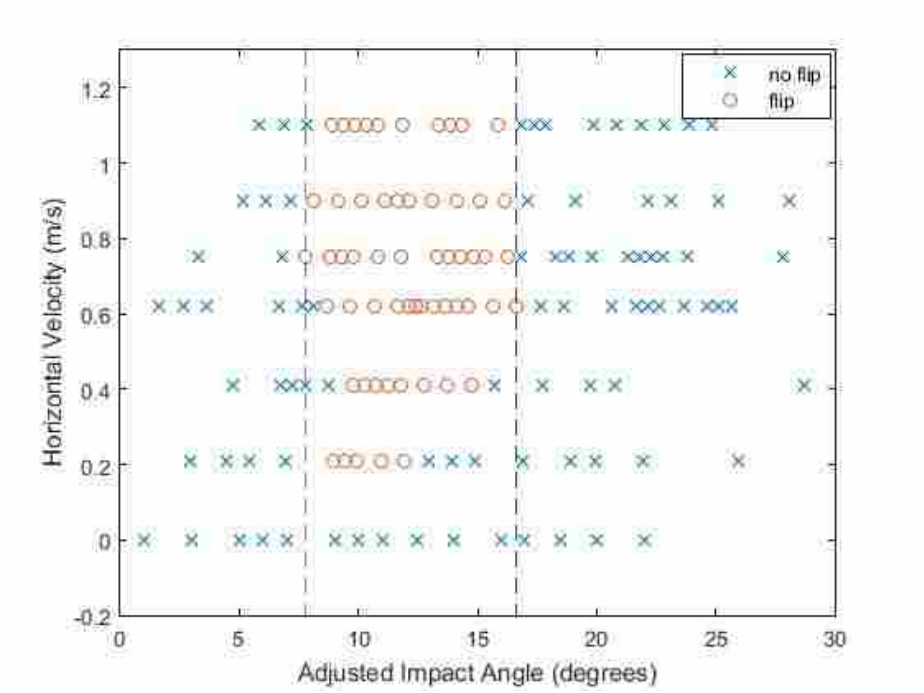

Figure 3.23: Adjusted inversion data for V_v=3.9 m/s using an adjusted impact angle (ϕ) which incorporates the trajectory angle. In this case $\zeta = 0.63$. Above a horizontal velocity of 0.6 m/s the graph collapses relatively well. However, below a horizontal velocity of 0.6 m/s it is unclear.

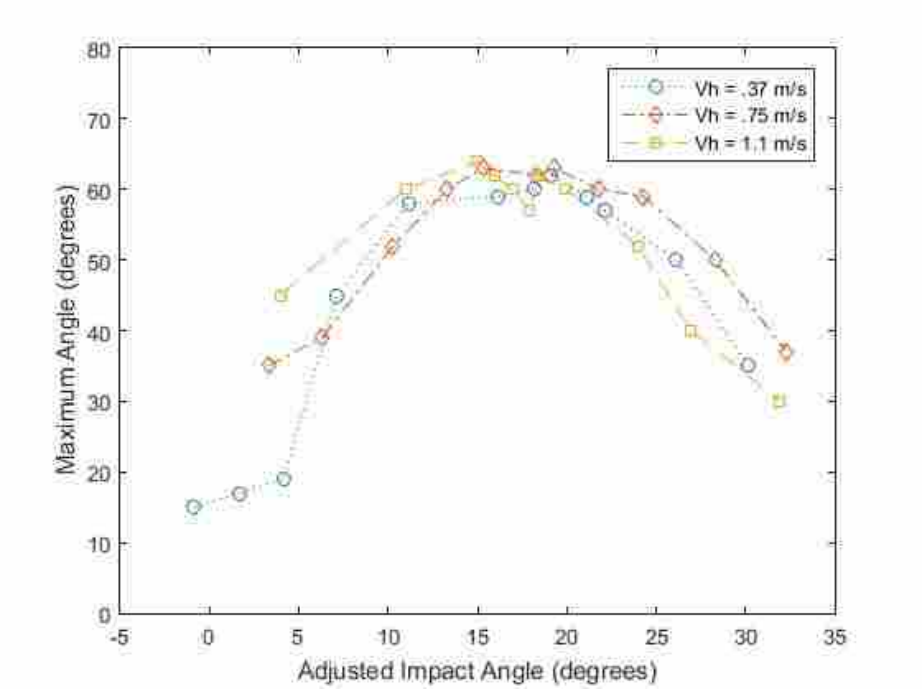

Figure 3.24: Adjusted maximum angle data for V_v=3.3 m/s using an adjusted impact angle (ϕ) which incorporates the trajectory angle. In this case $\zeta = 0.65$. The graphs come close together, but do not collapse perfectly onto one shape.

3.7 Nondimensional Comparisons to Previously Tested Geometries

The stability of an impacting object is highly dependant upon geometry. To date, three distinct shapes have been tested with the goal of determining inversion characteristics upon water impact. These three are the Apollo capsule, the Titan Mare Explorer (TiME) capsule as tested by Lorenz [26], and the buoyant cylindrical puck tested in this paper. A side by side comparison of these shapes is presented in Figure 3.25.

(a) (b) (c)

Figure 3.25: A side by side comparison of the three different shapes that have been tested for inversion characteristics. A cross section of the 1/4 scale Apollo command module [12] (a), the 1/8 scale TiME capsule [26] (b), and the cylindrical puck (c) are shown. The center of gravity is different in each case.

A clear distinction can be made between these shapes. The Apollo capsule is wider at the bottom than it is at the top, the TiME capsule is wider at the top than it is at the bottom, and the puck has an even diameter throughout. This difference in geometry affects the impact dynamics. Taking the two-dimensional cross sections illustrated in Figure 3.25, and assuming a typical (nose down) orientation at impact, a clear distinction arises. On the Apollo capsule, an acute angle impacts the water. On the TiME capsule, an obtuse angle impacts the water. On the puck, a right angle impacts the water. This difference in geometry intuitively means that the pitch angles at impact for which each capsule is likely to flip over is unique to the individual shape.

Another factor which affects inversion between these three geometrical shapes is the location of the center of gravity. The Apollo capsule's center of gravity is located slightly below the centerline as well as to the side of the geometric center. The TiME capsule's center of gravity is located at the center horizontally, but above the centerline vertically. The puck's center of gravity is directly in the center. The stability of an object an water is reduced when the center of gravity moves up or to the side. Even a small disturbance of an object in water with a center of gravity

above center applies an overturning moment. This must be counterracted by a shift in the center of buoyancy to remain upright. As a result, less energy is required to overturn an object with a center of gravity above the center.

Size in each case was scaled using the Froude number $Fr = V_i/\sqrt{gD}$. Stubbs did not directly mention the Froude number when he scaled the Apollo capsule for 1/4 scale tests. However, he gives a table of scaling factors which equate to using the Froude number [12]. Lorenz directly mentions using the Froude number to scale the TiME capsule [26]. A stability comparison these three shapes can begin to be approached by comparing the minimum Froude number at which inversion was seen in each case as seen in Table 3.1.

Table 3.1: Summary of inversion stability for the three object shapes which have been tested to date. The full-scale Apollo capsule is also included despite a limited number of tests.

Object	Diameter	Minimum V_i for inversion	Minimum Fr for inversion
1/4 Scale Apollo Capsule	0.96 m	4.6 m/s	1.5
1/8 Scale TiME Capsule	0.35 m	6.9 m/s	3.7
Buoyant Cylindrical Puck	0.083 m	3.91 m/s	4.34
Full-scale Apollo Capsule	3.9 m	9.9 m/s	1.6

These results suggest that the buoyant cylindrical puck was the most stable geometry tested. This effect is not entirely due to shape. Density and location of the center of gravity were different in each case. The 1/4 scale Apollo capsule showed similar results to the full-scale Apollo Capsule. This gives greater validity to the Froude number scaling that was used. The 1/8 scale TiME Capsule was closer in stability to the puck than the Apollo Capsule.

In each case, inversion characteristics depended upon an asymmetrical cavity that is formed upon water impact. Introducing a horizontal velocity at impact is one method of creating an asymmetrical cavity. This was noted for both the Apollo and the TiME capsules. Another method of creating an asymmetrical cavity is by introducing a pitch angle at impact. The range of pitch angles for which the given object was unstable shifted as horizontal velocity increased. Perhaps the most interesting difference between the three cases is that only the cylindrical puck flipped over consistently with no horizontal velocity. Tests of the 1/8 scale TiME capsule reported a critical hor-

izontal velocity of 1.2 m/s as can be seen in Figure 1.8. Below this value the capsule was expected to remain stable regardless of vertical velocity. However, one test did flip over at a lower horizontal velocity. This outlier was explained as having impacted at an extreme ($\sim 30^{\circ}$) pitch angle. This suggests a possibility that the range of angles for which the capsule will flip over at low horizontal velocities simply shifted to a range that would never be seen during typical tests for the TiME capsule. This is also a possible explanation for why extremely high horizontal velocities would not flip over. The range of impact angles for which the capsule will flip over at high horizontal velocities may have again shifted to a range that would never be seen during typical tests. This explanation would be more consistent with tests done for a cylindrical puck. However, this can not be determined for sure without additional tests.

The Apollo capsule also did not flip over for cases with no horizontal velocity. However, a very small sample size of vertical velocities was tested. It remains a possibility that the Apollo capsule would invert with no horizontal velocity if higher vertical velocities were tested.

The results collected for the buoyant cylindrical puck are comparable to results from the TiME capsule and the Apollo capsule. The cylindrical puck is the most stable shape that was tested. However, more data is needed for the Apollo capsule and the TiME capsule to determine to what extent the variance in stability is due to geometry and location of the center of mass.

CHAPTER 4. CONCLUSION

This thesis presented inversion data for a buoyant cylindrical puck. Vertical velocity, horizontal velocity, and pitch angle at impact were independently varied to identify the dependance of inversion on these parameters. All measurements were obtained using high-speed images. Inversion trends were identified which could be compared and help clarify trends previously seen in the Apollo and TiME capsules.

High-speed images reveal that the collapse of an asymmetrical cavity beneath the puck is the cause of inversion. This asymmetrical cavity can be formed by introducing a horizontal velocity at impact as has been seen clearly from previous work by Lorenz [26]. However, the present study also elaborates on the effect of pitch angle at impact. Introducing a pitch angle at impact causes an asymmetrical cavity to form even when no horizontal velocity is present.

As has been seen previously, the buoyant cylindrical puck used in this study would not flip over below a critical vertical velocity at water impact. The critical vertical velocity was slightly lowered when a horizontal velocity was introduced. As vertical velocity increased the puck tended to become more unstable and would flip over for a wider range of impact angles. The trends were supported by high-speed video which showed significantly less energy in the resulting cavity with lower vertical velocities. As a result, a smaller moment was applied to the puck when the cavity collapsed.

For the range of vertical velocities tested, increasing vertical velocity consistently decreased stability. However, if a high enough vertical velocity were tested, the cavity would actually collapse on top of the puck rather than underneath it. This offers the possibility that the puck may again be more stable at higher vertical velocities.

Each combination of vertical and horizontal velocity had a corresponding range of pitch angles at impact for which the puck was least stable. Some degree of symmetry is present when the pitch angle is either too high or too low. When the pitch angle is too low a cavity can form on

both sides of the puck resulting in a small moment applied during cavity collapse. A pitch angle that is too large will dive into the water without sitting back in the cavity. Upon cavity collapse, an insufficient moment is applied to flip the puck over.

The range of angles for which the puck was most unstable shifted towards lower angles as the horizontal velocity of the puck increased. With higher horizontal velocities, an asymmetrical cavity was still able to form at low pitch angles. The size of the range of angles for which the puck flipped over did not increase significantly as horizontal velocity increased. A small increase was noted, but was within experimental error.

Some tests flipped over for every horizontal velocity that was tested. An obvious limit to this is if the puck impacts with a high enough horizontal velocity that the puck would actually skip and leave the cavity before it collapsed. The transition between these regimes is uncertain without further testing; however, it is predicted that a gradual transition exists in which the collapsing cavity applies a smaller moment as the puck transitions to skipping.

The trends noted for a buoyant cylindrical puck give some insight into the limited data that we have for more complex shapes. The puck was shown to be more stable than either the Apollo or the TiME capsules. The Apollo capsule was the least stable, flipping over at Froude numbers below half of the value of the other two.

Several important factors that affect inversion are still not fully understood. Future work in this area could include the affect of the location of the center of mass. Moving the location of the center of mass down intuitively increases stability, but the extent to which is unknown at the present time. The Apollo command module was also significantly more stable in one orientation than another because the center of mass was off to one side. Moving the center of mass horizontally could also be explored.

Another factor for which there is limited data available is the shape of the impacting object. To date, only three shapes have been tested with varying degrees of depth. Testing more shapes in greater depth could help clarify the trends that have already been observed in previous studies. An embedded IMU could also be used to gain experimental data on acceleration experienced during inversion. Numerical studies that fully characterize inversion can also be attempted and verified as more experimental data becomes available.

REFERENCES

[1] Seddon, C., and Moatamedi, M., 2006. "Review of water entry with applications to aerospace structures." *International Journal of Impact Engineering,* **32**(7), pp. 1045–1067. 1, 8

[2] Benson, H. E., 1966. "Water impact of the apollo spacecraft." *Journal of Spacecraft and Rockets,* **3**(1), pp. 1282–1284. 2, 4

[3] Lorenz, R., 2011. "Apollo capsule capsize stability during splashdown: Application of a cavity collapse model." *Journal of the British Interplanetary Society,* **64**(1), pp. 289–295. 1, 3, 7, 8, 9, 29

[4] White, R. D. Apollo experience report: command module uprighting system Technical Memorandum D-7081, NASA, TN. 2, 4, 8, 9, 29

[5] Stofan, E., 1986. "Exploring the seas of titan: The titan mare explorer (time) mission." In *Lunar and Planetary Science Conference*. 2, 9

[6] Worthington, A. M. A study of splashes Longmans, Green, and Co. 3

[7] Karman, V. The impact of seaplane floats during landing Tech. Rep. 321, NACA, TN. 3

[8] Milwitzky, B. A generalized theory for seaplane impact Tech. Rep. 1103, NACA, TR. 4

[9] McGehee, J. Water-landing characteristics of a reentry capsule Tech. Rep. 5-23-59L, NASA. 4

[10] Thompson, W. C. Dynamic model investigation of the landing characteristics of a manned spacecraft Tech. Rep. D-2497, NASA, TN. 4

[11] Thompson, W. C. Dynamic model investigation of the rough water landing characteristics of a spacecraft Tech. Rep. D-3774, NASA, Washington DC. 4

[12] Stubbs, S. Dynamic model investigation of water pressures and accelerations encountered during landings of the apollo spacecraft Technical Memorandum D-3980, NASA, TN. 4, 5, 6, 7, 8, 42, 43

[13] Li, T., and Sigimura, T. Study of apollo water impact. volume 1–hydrodynamic analysis of apollo water impact final report Technical Memorandum NASA-CR-92019, North Aviation Inc., CA. 5

[14] Capelli, A., and Wilkinson, J. Study of apollo water impact. volume 2–dynamic response of shells of revolution during vertical impact into water Technical Memorandum NASA-CR-92020, North Aviation Inc., CA. 5

[15] Capelli, A., Salzman, R., and Wilkinson, J. Study of apollo water impact. volume 3–dynamic response of shells of revolution during vertical impact into water–hydroelastic interaction Technical Memorandum NASA-CR-92021, North Aviation Inc., CA. 5

[16] Wilkinson, J. Study of apollo water impact. volume 4–comparison with experiments final report Technical Memorandum NASA-CR-92022, North Aviation Inc., CA. 5

[17] Wilkinson, J. Study of apollo water impact. volume 5–final report Technical Memorandum NASA-CR-65860, North Aviation Inc., CA. 5

[18] Salzman, RN, W. J. Study of apollo water impact. volume 6–user's manual–interaction final report Technical Memorandum NASA-CR-65861, North Aviation Inc., CA. 5

[19] Capelli, A., and Furuike, S. Study of apollo water impact. volume 7–modification of shell of revolution analysis final report Technical Memorandum NASA-CR-92023, North Aviation Inc., CA. 5

[20] Capelli, A., Nishimoto, T., Pauley, K., and Radkowski, P. Study of apollo water impact. volume 8–unsymmetric shells of revolution analysis final report Technical Memorandum NASA-CR-92024, North Aviation Inc., CA. 5

[21] Capelli, A. Study of apollo water impact. volume 9–mode shapes and frequencies analysis Technical Memorandum NASA-CR-92025, North Aviation Inc., CA. 5

[22] Capelli, A., and Furuike, S. Study of apollo water impact. volume 10–users manual for modification of shell of revolution analysis final report Technical Memorandum NASA-CR-65862, North Aviation Inc., CA. 5

[23] Carrion, E., Furuike, S., and Nishimoto, T. Study of apollo water impact. volume 11–user's manual for unsymmetric shell of revolution analysis final report Technical Memorandum NASA-CR-65863, North Aviation Inc., CA. 5

[24] Wang, J., 2008. "Water landing analyses with explicit finite element method." In *in Proceedings of the 6th International Conference on Computation of Shell and Spatial Structures*. 8

[25] B.A. Tutt, A. T., 2004. "The use of ls-dyna to simulate the water landing characteristics of space vehicles." In *8th International LS-DYNA Users' Conference*. 8, 12

[26] Lorenz, R., 2015. "Inversion of a capsule impacting water: Flip by resurge jet." *Journal of Offshore Mechanics and Arctic Engineering,* **137**(4), p. 044501. 10, 11, 12, 25, 42, 43, 45

[27] Truscott, T., Epps, B., and Belden, J., 2013. "Water entry of projectiles." *Annual Review of Fluid Mechanics,* **46**. 10

[28] Rosellini, L., Hersen, F., Clanet, C., and Bocquet, L., 2005. "Skipping stones." *Journal of Fluid Mechanics,* **543**. 12

[29] Belden, J., Jandron, M., and Truscott, T., 2013. "Physics of elastic spheres skipping on water." *Physics of Sports*. 12

[30] Boef, W., 1992. "Launch and impact of free-fall lifeboats. part i impact theory." *Ocean Engineering,* **19**(2), p. 119. 12

[31] Boef, W., 1992. "Launch and impact of free-fall lifeboats. part ii implementation and applications." *Ocean Engineering,* **19**(2), pp. 139–159. 12, 13

APPENDIX A. ERROR ANALYSIS

Horizontal velocity was measured after each test by measuring a horizontal distance in pixels that the puck traveled and the number of frames it took to travel that distance. This was converted to m/s by using the known geometry of the puck and the known frame rate of the camera. In order to create cross-sections of the data, all tests run with the same motor settings were assumed to have the same horizontal velocity. The actual standard deviation on this horizontal velocity measurement ranged from 0.01 to slightly above 0.025 m/s with higher horizontal velocities having a larger variance. This number was approximately double what I would have expected had the error been due to the resolution of the images and the frame rate of the camera alone. In the interest of representing the true uncertainty, error is reported as plus or minus two standard deviations rather than calculating the standard error of the mean.

Impact angle was measured just prior to impact. The only error accounted for in this instance is the resolution of the images. It is estimated that pitch angle could be measured to the nearest degree. Error in impact angle is therefore estimated to be plus or minus 0.5 degrees. Measurement of maximum angle was slightly more complicated. Due to shifts in the perspective of the camera as well as small out of plane rotation, the error in maximum angle is estimated to be a much higher plus or minus 5 degrees.

Vertical velocity was calculated using the drop height neglecting drag. Neglecting drag was justified by estimating the drag force (F_D) at maximum velocities run in this experiment using $F_D = C_D \rho V^2 A/2$. The force due to gravity was found to be more than an order of magnitude larger than the counteracting force due to drag. There was some error in the measurement of drop height. It was estimated that the drop height could be off by as much as 0.5 inches which was based upon the size of the tab of aluminum foil. This resulted in a maximum error of plus or minus 0.05 m/s. Vertical velocity was also measured for a limited number of cases to test the validity of neglecting drag and found to fall within this proscribed error.

Angle and angular velocity were measured over time for one case. In this particular case a good side view was always available to measure the angle. The uncertainty in the angle measurement was estimated to be plus or minus 1 degree. The uncertainty in angular velocity was calculated using the propagation of uncertainty for a derivative ($\Delta_\omega = \frac{\partial \omega}{\partial \alpha}\Delta_\alpha$). This resulted in a maximum error of plus or minus 18 degrees per second.